HIGH STRAIN RATE MEASUREMENTS FOR PREDICTING BRAIN TRAUMA

A Thesis

Presented to the Faculty of the Graduate School

of Cornell University

in Partial Fulfillment of the Requirements for the Degree of

Master of Science

by

Mariana Tovar Torres

August 2025

ABSTRACT

Soft, high-speed sensors are crucial for real-time detection of mechanical deformation in brain-like materials, particularly in studying mild traumatic brain injury (mTBI). This work presents the design, fabrication, and validation of stretchable optical fiber sensors using thermoplastic polyurethane waveguides paired with infrared optoelectronics. A repeatable process was established, producing sensors with consistent mechanical stiffness and electrical sensitivity under tensile loads. Dynamic testing was performed using ballistic and blunt impacts in hydrogel, silicone, and preserved sheep brain tissue. Results confirmed millisecond-scale responsiveness and sensitivity to both local deformation and impact propagation. Sensor performance under compressive and constrained conditions was also evaluated, revealing limitations due to pre-strain and material swelling. A localization framework based on LASSO regression was developed and validated on a 2D sensor matrix. While complete 3D localization was not implemented, the system demonstrated feasibility for integration into future diagnostic platforms for mTBI detection and soft-tissue impact sensing.

BIOGRAPHICAL SKETCH

Mariana was born and raised in Mexico City. She earned a B.S. in Mechanical and Electrical Engineering from Universidad Iberoamericana before completing a MicroMasters in Probability, Statistics, and Data Science at MIT. She is currently pursuing an M.S. in Mechanical Engineering at Cornell University, where she focuses on control systems, biomechanics, and sensor technology.

Before graduate school, she worked in the automotive industry, including a role in the armored vehicle division as Chief of the division and multiple internships at BMW in Germany and the USA, where she contributed to the Data Analytics and Digitalization and the Technical Planning team. These experiences strengthened her background in engineering design, system integration, and data-driven analysis.

At Cornell, her research focuses on developing an optical sensor network for modeling mild traumatic brain injury (mTBI). Using thermoplastic polyurethane (TPU) optical fibers, the sensors detect changes in light intensity caused by mechanical deformation, enabling high-speed displacement and strain measurements. This system is designed to improve understanding of tissue-level injury mechanisms and advance diagnostic capabilities for mTBI.

She is passionate about applying her expertise in sensor technology and biomechanics to real-world challenges. Looking ahead, she aims to contribute to research and development in an international setting, working on innovative solutions at the intersection of engineering and human health.

To my family and friends, their unconditional support and encouragement.

To my father, Thank you for teaching me that curiosity is a strength And that dreams are worth chasing, even when the path is unclear.

And to the version of me who kept going, for having the stubborn bravery and foolish tenacity to see this through.

ACKNOWLEDGEMENTS

There's no such thing as doing research alone—not the kind that has you tweaking sensors for the hundredth time, hitting dead ends, and still finding a reason to try again.

To the faculty and staff at Cornell University, thank you for creating an environment where curiosity is supported and ideas are allowed to grow.

I want to thank Dr. Robert Shepherd for the opportunity to join the Organic Robotics Lab and for the trust and support to explore this project in my own way.

My deepest thanks go to Dr. Anastasia Koivikko, who has been both a mentor and a friend. This thesis wouldn't exist without her. From the start to the very end, she's been there—offering clarity, encouragement, and unwavering support. She made the failures more bearable and the successes all the more exciting. This thesis is as much hers as it is mine.

To everyone in ORL—Chan, Young, Khoi, Doug, Ofek, June, and Pranandu, and April—thank you for making the lab a space that always felt collaborative. I am glad to have had the opportunity to build, break, and brainstorm with you.

To my friends Devin, Justin, Falak, LZ, and Heather, who made this work and my experience at Cornell unforgettable, and helped me to create memories and friendships that will last for a lifetime.

To Chris, thank you for showing up every day, especially on the hard ones. For all the late nights, the pep talks, and the way you stayed close even when things got messy. This road was brighter with you walking beside me.

And finally, to my parents, Armando and Nimbe, and my sister Tania—thank you for being behind me in every way that counts. This degree may have my name, but it belongs to you, too.

TABLE OF CONTENTS

LIST OF TABLES

LIST OF FIGURES

LIST OF ABBREVIATIONS

Abbreviation	Definition
2D	Two-Dimensional
3D	Three-Dimensional
ADC	Analog-to-Digital Converter
CAD	Computer-Aided Design
DAQ	Data Acquisition System
FBG	Fiber Bragg Grating
SLIMS	Stretchable Lightguide for Multimodal Sensing
Hz	Hertz
IR	Infrared
LASSO	Least Absolute Shrinkage and Selection Operator
LED	Light-Emitting Diode
mTBI	Mild Traumatic Brain Injury
N, N/mm	Newton, Newtons per Millimeter
NI	National Instruments
PDMS	Polydimethylsiloxane
SNR	Signal-to-Noise Ratio
s.d., σ	Standard Deviation
TBI	Traumatic Brain Injury
TIA	Transimpedance Amplifier
TPU	Thermoplastic Polyurethane
UV	Ultraviolet
V, V/mm	Volt, Volts per Millimeter
Δ	Voltage Change (Difference between Max and Min per cycle)

Table 1: List of Abbreviations used throughout the thesis

PREFACE

Soft, high-speed sensors are essential for the real-time detection of mechanical deformation in brain-like materials, particularly in the study of mild traumatic brain injury (mTBI). This work presents the design, fabrication, and validation of stretchable optical fiber sensors made from thermoplastic polyurethane waveguides, paired with infrared optoelectronics. A repeatable process was established to produce sensors with consistent mechanical stiffness and electrical sensitivity under compression loads. Dynamic testing was conducted using ballistic and blunt impacts on hydrogel, silicone, and preserved sheep brain tissue. The results confirmed that the sensors responded within milliseconds and demonstrated sensitivity to both local deformation and the propagation of impacts. Additionally, the performance of the sensors under compressive and constrained conditions was evaluated, revealing some limitations due to pre-strain and material swelling. A localization framework based on LASSO regression was developed and validated on a 2D sensor matrix. While complete 3D localization was not yet implemented, the system showed promise for integration into future diagnostic platforms for mTBI detection and soft-tissue impact sensing.

CHAPTER 1

INTRODUCTION

1.1 Motivation and introduction to TBI and mTBI

Traumatic brain injury (TBI) is one of the leading causes of fatality and disability worldwide, with mild TBI (mTBI), commonly referred to as concussion, being particularly difficult to detect and monitor in real time. These injuries can arise from a wide range of scenarios, such as sports-related impacts, military blast exposure, or accidents on construction sites. Although some symptoms of mTBI, such as cognitive fog or depression, may appear subtle, they can have lasting neurological consequences if left untreated. Unfortunately, current diagnostic approaches often rely on subjective reporting and imaging modalities that lack temporal resolution or sensitivity to dynamic mechanical events.

There is an increasing demand for real-time, wearable, and tissue-compatible sensor systems that can detect rapid mechanical deformation and help clinicians evaluate impact severity and location. Optical fiber-based soft sensors represent a promising avenue, offering high-speed response, flexibility, and minimal electromagnetic interference. This thesis investigates the development of such a sensor platform, aimed at modeling mTBI dynamics and laying the groundwork for future diagnostic tools.

1.1.1 Background and Challenges of Current Diagnostic Technology

Traditional methods of diagnosing TBI involve neurological evaluations, imaging (e.g., MRI or CT scans), and patient interviews. However, these techniques are generally employed after symptoms appear, which may not capture the immediate biomechanical event that triggered the injury. Moreover, some forms of mTBI can go undetected due to the absence of visible structural damage. This gap highlights the need for real-time mechanical monitoring systems, particularly in high-risk environments [[13],[19]]. Soft and stretchable sensors have emerged as key enabling technologies in biomechanics and wearable electronics.

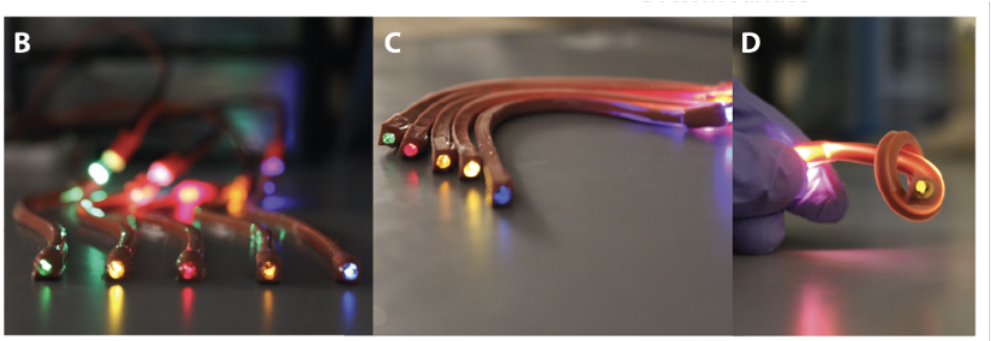

Figure 1.1: Fabricated stretchable optical waveguides demonstrating flexibility and light transmission: (B) waveguides with LEDs of assorted colors in a sinuous arrangement, (C) curved configuration, and (D) waveguide tied into a knot.[1]

[1] Note. Adapted from Zhao, H., Li, Y., Mao, Y., Sun, J., Shepherd, R. F. (2016). Optoelectronically innervated soft prosthetic hand via stretchable optical waveguides. *Science Robotics*, 1(1), eaai7529.

Optical sensors, particularly those based on stretchable optical waveguides,

offer fast response times and the ability to conform to irregular surfaces [25],[26]. Despite this promise, few systems have demonstrated the ability to detect high-speed impacts (¿250 kHz) in soft tissue-like environments [1]. In parallel, experimental models of TBI are typically limited by their mechanical complexity or lack of modular sensor integration. Animal models and weight-drop setups offer biological relevance but low repeatability, while in vitro gel-based setups often lack anatomical realism [5],[15]. Thus, there is a clear opportunity to merge high-speed soft sensing with controllable, anatomically inspired platforms.

1.1.2 Objectives

The central objective of this thesis is to design, fabricate, and evaluate a stretchable optical fiber sensor platform capable of detecting mechanical impacts relevant to mTBI. The project also aims to integrate the sensors into synthetic and biological models to assess their performance across a range of media and loading conditions. Specific goals include the development of a repeatable sensor fabrication method for optical strain sensors; the characterization of the mechanical and electrical behavior of the sensors under compression and impact; the embedding of sensors into synthetic soft materials (hydrogel and silicone) and preserved brain tissue; the evaluation of dynamic sensor responses under high-speed loading conditions; and the exploration of preliminary spatial localization using LASSO regression models.

1.1.3 Contributions of Present Work

This work presents the development and evaluation of a novel high-speed optical sensing platform for soft-tissue impact detection. A robust fabrication protocol was established for soft optical fiber sensors, demonstrating both mechanical and electrical repeatability across multiple samples. In addition, the sensors were embedded in both 2D and multilayer soft material arrays. Early hydrogel tests supported optical signal transmission without cladding, while the later transition to silicone required optical confinement strategies such as cladding using ELASTOSIL® RT 604. These arrays were used to evaluate signal propagation, localization potential, and sensor durability under repeated impacts. The sensors were then successfully integrated into preserved sheep brain tissue, both on the surface and within tissue, with and without cranial constraints. These biological tests provided valuable insights into sensor behavior in anatomically relevant settings, including unexpected phenomena such as fiber swelling and saturation under hydrated conditions. The final contribution involved the development of a MATLAB-based localization framework using LASSO regression. This method was tested on a 2D matrix of 24 sensors, enabling the mapping of voltage responses into spatial heatmaps of localized impact. Although the 3D extension of this model was not implemented due to hardware constraints, the successful application of LASSO in 2D lays a viable foundation for future real-time localization models.

1.2 Structure of the Thesis

The remainder of this thesis is organized as follows:

- **Chapter 2:** Background and Literature Review
- **Chapter 3:** Sensor Design, Fabrication, and Calibration
- **Chapter 4:** Sensor Array Development and Material Integration
- **Chapter 5:** Mechanical Testing and Impact Response Characterization.
- **Chapter 6:** High-Speed Impact Testing on Synthetic Models.
- **Chapter 7:** Sensor Integration and Testing on Biological Models.
- **Chapter 8:** Conclusion and Future Work

CHAPTER 2

BACKGROUND AND LITERATURE REVIEW

2.1 Traumatic Brain Injury: Definition, Mechanisms, and Challenges

Traumatic brain injury (TBI) refers to any disruption in normal brain function caused by an external mechanical force. TBI can range from mild injuries, such as concussions, to severe, life-threatening trauma. Mild traumatic brain injury (mTBI), while often perceived as less serious, can lead to cognitive, emotional, and physical impairments that persist long after the initial injury [8]. One of the primary challenges associated with mTBI is its subtle presentation; many cases go undiagnosed or are diagnosed late, which increases the risk of cumulative damage and long-term neurological decline [12].

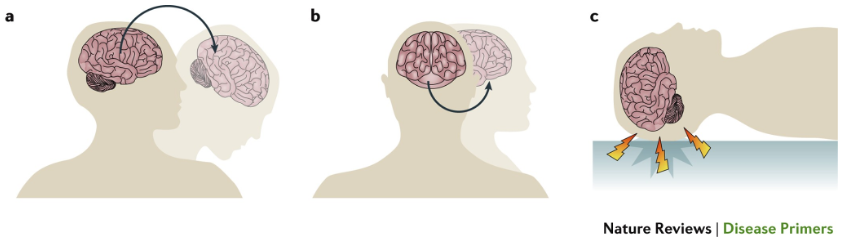

Figure 2.1: Examples of the types of forces in mild traumatic brain injury. (Nature, "Traumatic brain injuries")

Mechanically, TBI can arise from various pathways, including linear acceleration, rotational acceleration, and the transmission of pressure waves through the skull and into the brain tissue [17]. These forces can cause strain, compression, and shear within the soft brain matter, potentially disrupting neural pathways and damaging blood vessels at a microscopic level. Of particular concern

are rotational forces, which have been increasingly recognized as particularly damaging, often resulting in diffuse axonal injury—a hallmark of mTBI [24].

Traditional diagnostic methods predominantly rely on imaging techniques such as magnetic resonance imaging (MRI) and computed tomography (CT). However, these modalities have limitations in detecting the microscopic or biochemical changes associated with mild injuries [20]. As a result, many mTBIs are diagnosed based mainly on clinical symptoms and patient-reported outcomes, introducing an element of subjectivity and leading to delays in diagnosis. This diagnostic gap highlights the critical need for systems that can capture mechanical events in real time, ideally providing early indicators of tissue-level strain and deformation that could lead to injury.

2.2 Current Sensing Technologies for Head Impact Detection

Efforts to monitor head impacts have mainly focused on external measurement techniques, particularly through the use of wearable sensors integrated in helmets or mouthguards [24]. These devices typically employ accelerometers, gyroscopes, or pressure sensors to infer the severity of impacts by tracking head kinematics. While they provide valuable data regarding translational and rotational accelerations, they do not directly measure the internal mechanical environment of the brain [14]. Instead, they estimate the potential for injury based on thresholds derived from external forces, which may not fully capture the complexities of individual tissue responses.

Accelerometer-based systems, such as the Blast Gauge sensor utilized in military applications, offer portability and expedite data acquisition; however, they

are confined to measuring skull-level motion [**blastgauge˙device**]. More sophisticated systems aim to reconstruct forces at the brain level through modeling techniques, yet these approaches remain indirect and are often subject to significant uncertainties. Furthermore, many current sensors have a limited bandwidth, often capturing signals only up to a few kilohertz, which is inadequate to resolve the rapid and transient events associated with ballistic or blunt trauma [21].

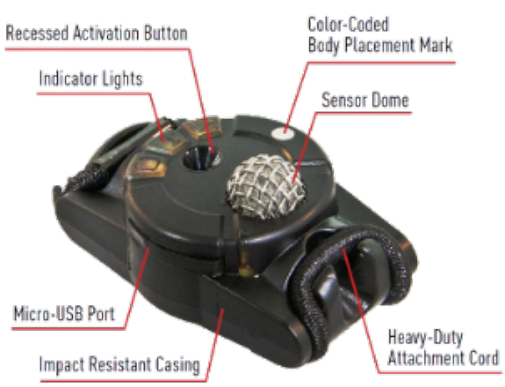

Figure 2.2: Blast Gauge sensor designed to monitor blast overpressure events in field environments, aiding in the assessment of TBI risk. Adapted from Blast Gauge System, by BlackBox Biometrics, n.d. (https://blastgauge.com). Copyright by BlackBox Biometrics. Used under fair use for educational purposes.

Recent developments in stretchable strain sensors, including resistive, capacitive, and optical systems, have begun to mitigate some of these limitations [7]. While resistive and capacitive sensors are flexible, they are also susceptible to electrical noise, environmental fluctuations, and mechanical fatigue. In contrast, optical fiber sensors, particularly those that detect changes in light transmission rather than relying on electrical signals, offer an appealing alternative due to their mechanical compliance and immunity to electromagnetic interference. However, integrating these sensors into three-dimensional, deformable structures like brain tissue models remains a relatively untapped area, representing a significant opportunity for innovation.

Table 2.1: Sensor Comparison Table with TBI Compatibility

Fabrication Method	Materials	Stretchability (%)	Hysteresis (%)	Sensing Type	Gauge Factor (GF)	TBI/Bio Model Compatible?
Cladding on TPU	TPU fiber, IR LED + photodiode	[1]	90[1]	Optical (intensity)	[1]	Yes
Drawn silica fiber + grating inscribing	Silica fiber with Bragg grating	1[2]	¡1[2]	Optical (wavelength shift)	¿1000[2]	No
Screen-printing	Graphene/CNT in silicone	100[3]	10–30[3]	Resistive	50–5000[3]	Limited
Microchannel casting	eGaIn in silicone elastomer	300[4]	~5[4]	Resistive	2–10[4]	Limited
Soft lithography	ZnO-doped silicone, hydrogel	490[5]	¡2[5]	Capacitive	0.7[5]	Limited
Commercial polymer composite	Bend sensor (Flex®)	¡10[6]	10–13[6]	Resistive	7–40[6]	No
Photolithography + bonding	Silicone waveguide + photodetectors	100[7]	3–10[7]	Optical (intensity)	5–15[7]	Yes

Note. Superscript numerals indicate sources:
[1] Zhao et al., *Sci. Robot.*, 2016
[2] Kersey et al., *J. Lightwave Technol.*, 1997
[3] Amjadi et al., *Adv. Funct. Mater.*, 2016
[4] Park et al., *Nat. Mater.*, 2012
[5] Trung & Lee, *Adv. Mater.*, 2016
[6] Flexpoint Sensor Systems, 2024
[7] Yang et al., *Sci. Adv.*, 2023

2.3 Fiber Optic Sensing: Principles and Advantages

Fiber optic sensors operate by guiding light through a dielectric waveguide, typically made of polymer or glass fiber. Changes in the surrounding environment modulate the intensity, phase, or wavelength of the transmitted light. In this study, intensity-modulated fiber optic sensors were used. These sensors detect mechanical deformations, such as stretching, bending, or compression, which alter the light intensity reaching the photodetector.

The core optical principle behind these sensors is total internal reflection

(TIR). When light enters the fiber core, it propagates by repeatedly reflecting off the core-cladding interface. TIR occurs when light traveling in a medium with a higher refractive index (n_1, representing the core) strikes the boundary with a lower refractive index medium (n_2, representing the cladding) at an angle greater than the critical angle (θ_c), which can be expressed as:

$$\theta_c = \arcsin\left(\frac{n_2}{n_1}\right) \tag{2.1}$$

For the fibers used in this work, the core and cladding refractive indices were approximately $n_1 = 1.53$ and $n_2 = 1.43$, respectively. Substituting these values gives:

$$\theta_c = \arcsin\left(\frac{1.43}{1.53}\right) \approx 69.17^\circ \tag{2.2}$$

As long as this condition is maintained, the light remains trapped within the core. However, when the fiber is externally deformed, such as through bending, the local incident angle of the light rays within the waveguide can change. If this bending reduces the incident angle below θ_c, some light can escape the core and be lost to the surrounding medium. This loss is perceived as a drop in optical power (P), which can be quantified at the photodiode [**ghatak˙fiberoptics**].

For macro bending loss, the relationship between the bend radius (R) and power attenuation (α) can be approximated as:

$$\alpha(R) \propto \exp\left(-\frac{C \cdot R}{\lambda}\right) \tag{2.3}$$

where λ represents the wavelength of the light, and C is a constant [**marcuse˙fiberloss**] dependent on the material.

Similarly, stretching the fiber leads to changes in its optical path length and cross-sectional geometry, which reduces confinement efficiency and increases scattering or leakage [16]. Intensity-modulated fiber optic sensors are simple to fabricate and interrogate. Unlike fiber Bragg gratings (FBGs) or interferometric sensors, which require precise alignment and spectrally sensitive readout systems, intensity-based sensors utilize only a photodiode to convert light into voltage. This significantly reduces costs, complexity, and space requirements, making the system scalable for distributed networks [22].

In applications such as research on mild traumatic brain injury (mTBI), these sensors provide additional advantages. Their small size, mechanical flexibility, and compatibility with soft substrates allow them to be integrated into synthetic brain models and biological tissue [11]. Their high temporal resolution—limited only by the rise time of the photodiode and data acquisition system—enables the capture of rapid strain events, including ballistic impacts [23].

Moreover, since their operation is entirely optical, these sensors are immune to electromagnetic interference and pose no electrical hazard to biological tissue. This is particularly significant in clinical or wearable applications. The combined attributes of mechanical compliance, speed, and safety make intensity-based optical sensors highly attractive for dynamic, high-resolution strain monitoring in soft matter and biomedical systems.

[2] Adapted from Fig. 1C in Xu et al. (2020), .

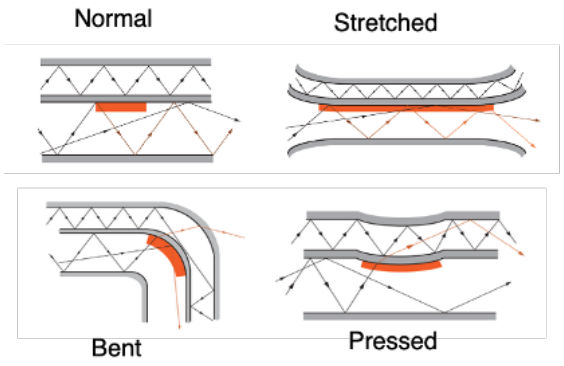

Figure 2.3: Optical outputs and ray diagrams of SLIMS under various deformations, illustrating light reflection on the TPU fiber during mechanical deformation.[2]

2.4 Brain-Mimicking Materials: Hydrogel and Silicone Composites

Effective modeling of the brain's mechanical environment requires materials that replicate its distinctive combination of softness, viscoelasticity, and water content. Hydrogels, mainly composed of water and cross-linked polymer networks, have been used extensively to simulate brain tissue due to their similar mechanical properties [9]. Substances such as agarose, gelatin, and poly(ethylene glycol) diacrylate (PEGDA) can be adjusted to match the elastic modulus of brain tissue, which typically ranges from 0.1 to 10 kPa [2].

In the initial stages of this project, hydrogels were employed to embed optical fiber sensors. Their mechanical resemblance to brain tissue facilitated the examination of stress wave propagation following impact events. However, practical challenges soon arose. Hydrogels were susceptible to dehydration over time, resulting in alterations to their mechanical properties and introducing signal artifacts. Moreover, concerns regarding microbial contamination and struc-

tural fragility limited their effectiveness for extended experimental applications.

To overcome these challenges, the project shifted to silicone-based composites. Silicone elastomers, such as Dragon Skin and Ecoflex, present a stable and durable alternative that can be finely tuned to approximate the mechanical behavior of brain tissue while ensuring structural integrity over prolonged periods. Silicone allows for improved handling during high-speed impact tests and enables repeated trials without material degradation. Although it does not replicate the brain's water content, its consistent mechanical performance made it the preferred medium for constructing multilayer sensor arrays and conducting ballistic impact experiments.

2.5 Biological Models for Brain Impact Testing

While synthetic materials provide controlled environments for sensor testing, biological tissues offer a closer approximation to the human brain's real mechanical and anatomical conditions. Animal models, particularly sheep brains, have been extensively used in TBI research due to their anatomical and biomechanical similarities to the human brain [18]. Sheep brains exhibit comparable cortical folding, elasticity, and structural layering, making them valuable for studying impact responses. In this research, an ex vivo sheep brain model was employed to test the integration of the optical sensor network into a biological substrate. Sensors were attached directly to the brain surface, and tapping experiments were conducted to simulate low-force impacts. This approach allowed for the evaluation of sensor responsiveness in a living tissue analog, highlighting issues such as intracranial pressure artifacts when sensors

are compressed within confined spaces like the skull. Although challenges remain in achieving perfect sensor-tissue coupling, these experiments represent a critical step toward validating the system's performance in physiologically relevant conditions.

CHAPTER 3

SENSOR DESIGN, FABRICATION AND CALIBRATION

3.1 Optical Sensor Design and Working Principle

The optical fiber sensors developed for this project consist of three main components: an infrared light-emitting diode (LED), a stretchable thermoplastic polyurethane (TPU) optical fiber, and a silicon PIN photodiode. The LED emits infrared light that propagates through the optical fiber via total internal reflection, and the photodiode detects the transmitted light intensity at the opposite end. When the fiber undergoes mechanical deformation from tension, compression, or bending, the light transmission is altered due to geometry, surface contact, or scattering changes. The corresponding voltage change at the photodiode provides a direct electrical signal proportional to mechanical strain [27].

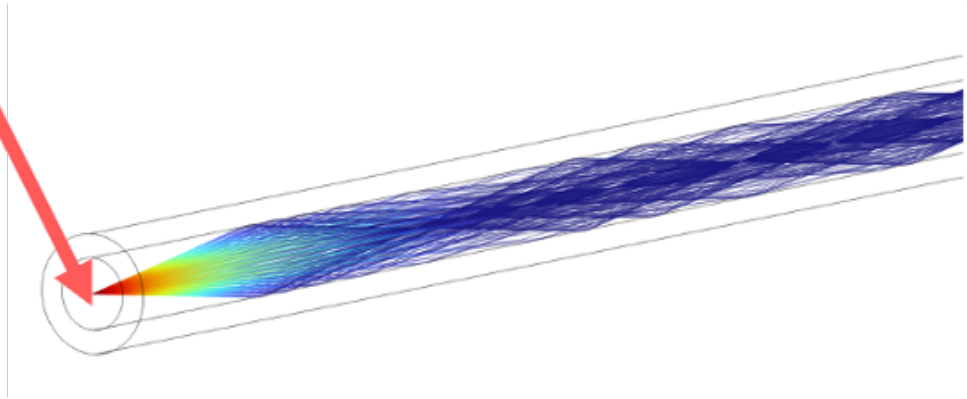

Figure 3.1: Schematic of the optical sensor showing the LED, optical fiber, and photodiode with the light propagation path using COMSOL software.

$$\theta_c = \arcsin\left(\frac{n_{\text{cladding}}}{n_{\text{TPU}}}\right) = \arcsin\left(\frac{1.43}{1.53}\right) \approx 69.17^\circ$$

$$n_{\text{TPU}} \approx 1.53 \quad \text{(polyurethane)}$$

$$n_{\text{cladding}} \approx 1.43 \quad \text{(silicone)}$$

The basic principle relies on total internal reflection (TIR), which Snell's law governs. The condition for TIR in a core-cladding system is given by: Where:

- is the refractive index of the TPU optical fiber core,
- is the refractive index of the ELASTOSIL® RT 604 cladding layer.

This equation emphasizes the requirement $n_{\text{cladding}} < n_{\text{core}}$ to maintain internal light transmission within the fiber. These analog voltage signals are captured using a high-speed 32-channel data acquisition (DAQ) system, capable of sampling rates up to 500 kS/s.

3.2 Sensor Fabrication Process

The sensors were fabricated using a standardized procedure to ensure consistency and repeatability. TPU optical fibers (Crystal Tec Korea), available in diameters of 0.6 mm and 1.0 mm, were cut to a length of 11.25 cm, with their ends cut to a precise 90-degree angle. Initially, 0.6 mm fibers were utilized due to their smaller profile and flexibility. However, subsequent iterations favored the 1.0 mm fibers, which offered improved optical transmission, reduced cladding instability, and enhanced handling ease during fabrication.

To optimize optical coupling, a 2 mm orifice was drilled at the center of both the LED and the photodiode using a 5 mm drill bit. The optoelectronic compo-

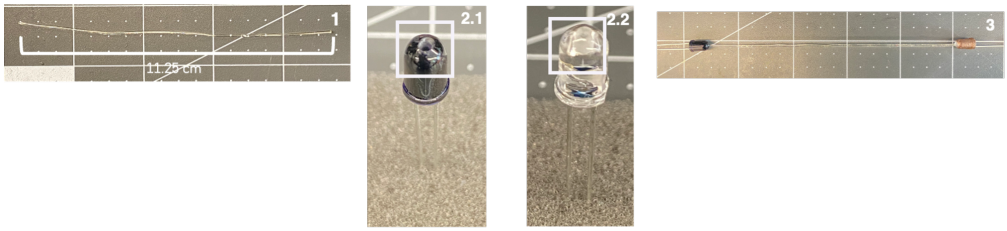

Figure 3.2: Step-by-step illustration of the sensor fabrication process. 1. Indicates the length of the TPU fiber, 2.1. and 2.2. Highlight the 2 mm orifice on each optoelectronic, and 3 shows the whole attachment of the parts as a complete sensor.

nents and fiber ends were affixed with optically clear Loctite glue, with particular attention paid to eliminating air bubbles that could disrupt transmission. The sensors were cured under ambient pressure in a horizontal orientation for at least 24 hours. No post-processing or additional polishing was performed after curing to maintain the integrity of the fiber's surface and prevent further misalignment. This modular design enabled easy replication, and eight sensors were batch-fabricated for consistency tests.

Parameter	Value	Tolerance
Fiber Length	11.25 cm	±0.5 mm
Drill Hole Depth	2.0 mm	±0.5 mm
Cut Angle	90°	–
Fiber Diameter	0.6 mm or 1 mm	–

Table 3.1: Fabrication Parameters and Tolerances

3.3 Embedding Sensors into Soft Materials

Single sensors were embedded into two soft materials: transparent hydrogels and opaque silicone elastomers. The goal was to characterize performance in different matrix conditions. Hydrogel embedding uses pre-cast rectangular molds filled with a 1:3 mixture of 6% Gelatin and 0.6% Agarose hydrogels.

Sensors were suspended mid-volume and fixed at both ends to maintain pre-strain. These tests confirmed a clear signal transmission due to high optical transparency [14].

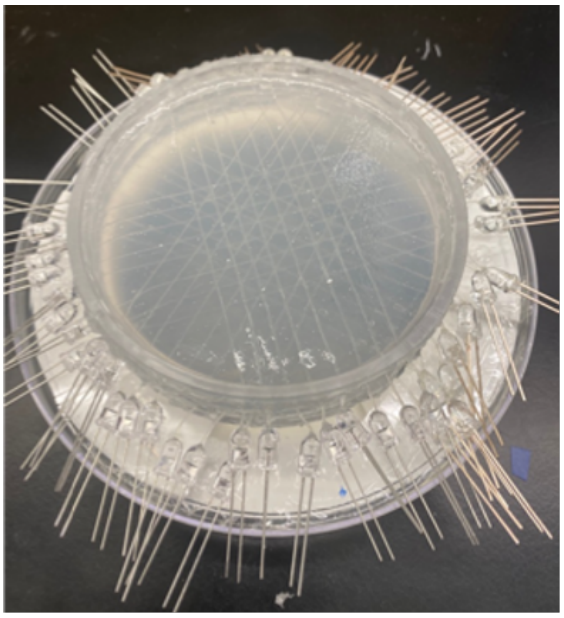

Figure 3.3: Hydrogel embedded with sensor array on circular model.

In contrast, silicone models were cast using Ecoflex 00-30, a platinum-cured silicone with mechanical properties similar to brain tissue. The opaque nature of this material caused light scattering and loss of signal, which led to the development of optical fiber cladding.

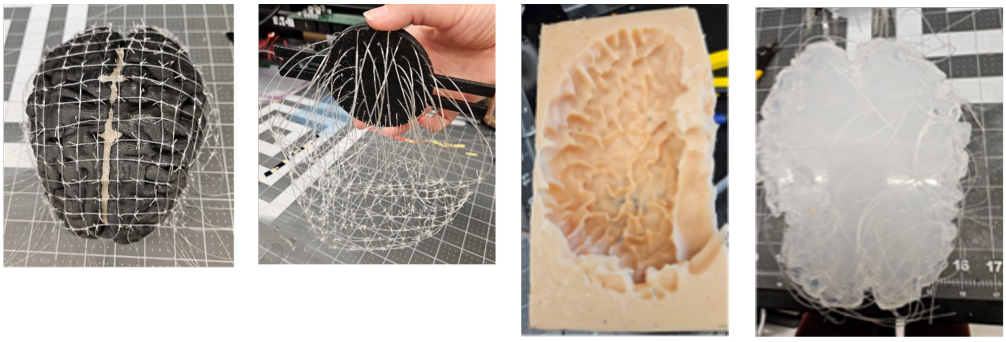

Figure 3.4: Process showing how the network of fiber was embedded into the silicone mold to cast it with Ecoflex 00-30. A) Shows the "grid" of TPU fibers

The cladding was applied using Wacker ELASTOSIL® RT 604 A/B, an optically clear silicone. This coating formed a lower-index sheath around the TPU core, promoting total internal reflection. Rayleigh instability—visible as pearling along the fiber length was initially a problem, especially on thinner 0.6 mm fibers. Switching to thicker 1.0 mm fibers significantly improved uniformity due to the larger surface area resisting curvature instabilities [10]. The larger diameter also improved light transmission, reducing losses due to scattering and enhancing signal strength at the photodiode.

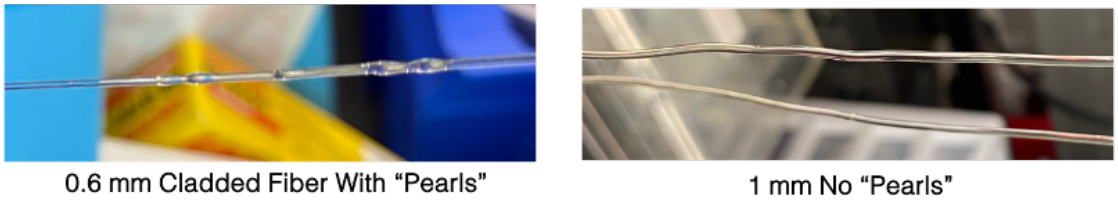

(a) Cladding with Pearls (b) Cladding with No Pearls

Figure 3.5: Comparison image showing cladded 0.6mm fiber (with pearling) vs. smooth 1.0mm cladded fiber.

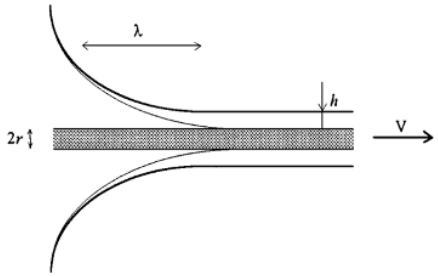

Figure 3.6: Rayleigh instability: when a liquid column breaks into droplets due to surface tension and small surface waves growing over time

3.4 Sensor Calibration and Adjustment

Once fabricated, each sensor required careful calibration to ensure consistent baseline voltage and responsiveness. The primary calibration involved tuning the LED output using 10 Ω potentiometers wired in series with the LED's power supply. This allowed for fine control of the light intensity transmitted through the fiber. Each sensor was powered and stabilized before tuning, and the potentiometer was adjusted so that the photodiode's voltage output was within an optimal operating range, typically between 1.5 V and 4.5 V, avoiding signal saturation and excessively low voltages. This range was selected to maintain headroom for detecting tensile and compressive strain variations. During the early stages of experimentation, it became evident that sensor behavior could drift due to minor inconsistencies in optical alignment or environmental light contamination. As a result, shielding strategies were implemented. A thin coat of metallic shielding paint was applied around the photodiode housings to prevent ambient light interference and optical crosstalk between adjacent sensors in array configurations. This approach was introduced during early tests with the hydrogel arrays and retained in all later iterations. The potentiometer-based

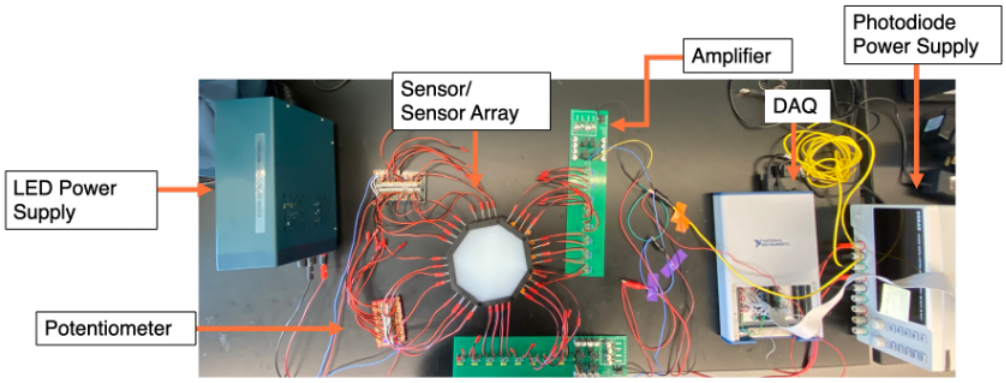

Figure 3.7: Electrical calibration schematic showing potentiometer circuit and voltage readout

tuning and shielding methods provided a repeatable and adjustable calibration procedure. They ensured that each sensor operated within a controlled voltage window and could reliably respond to dynamic loading scenarios across the various testing configurations described later in the thesis.

3.5 Validation Under Controlled Loading

Control tests were performed using a standardized compression protocol to validate the consistency and functionality of the fabricated optical fiber sensors. These tests were not intended to characterize material properties but to confirm reproducible sensor behavior under defined mechanical conditions. Four individual sensors were tested across five loading cycles using a 3D-printed cylindrical probe and a vertically adjustable stage. Voltage output was recorded via a transimpedance amplifier and DAQ system during incremental compressive displacements up to 0.3 mm. All sensors exhibited consistent signal trends with no evidence of saturation or mechanical degradation. This validation phase served as a baseline protocol before sensor integration into complex soft material models and biological tissues. It confirmed the repeatability, linear response, and electrical stability necessary for subsequent high-speed and embedded testing scenarios.

Parameter	**Observation**	**Outcome**
Voltage Range Stable	Yes (1.5–4.5V)	Passed
Linearity Observed	Yes (Force–Displacement)	Passed
Crosstalk Absent	Yes (With shielding)	Passed

Table 3.2: Sensor Validation Checklist

While Chapter 5 includes a more detailed analysis of these test results, in-

cluding force and voltage measurements, this section establishes that the sensors provided reliable outputs under controlled test conditions, justifying their use in subsequent experiments.

3.6 Performance Evaluation Criteria

To ensure consistent interpretation of sensor behavior across different materials and testing configurations, several criteria were used to evaluate sensor performance. First, the signal amplitude was monitored to confirm that the voltage response to mechanical stimuli was within the expected operational range of the photodiode-LED pair (typically 0–5V). Responses near the upper or lower limits were flagged as possible saturation artifacts. Second, the response time between mechanical impact and peak voltage change indicated system responsiveness, with sub-millisecond resolution indicating successful high-speed detection. Third, signal stability was assessed by monitoring the baseline drift and noise before and after impacts; stable pre- and post-impact voltages were considered favorable. Finally, repeatability was evaluated by repeating identical loading protocols on multiple sensors and noting the amplitude, waveform, and recovery consistency. A sensor was considered to perform reliably if it met acceptable ranges across these four domains. These benchmarks formed the basis for identifying limitations and validating performance across all.

CHAPTER 4

DEVELOPMENT OF SENSOR ARRAYS AND EMBEDDING ARCHITECTURES

4.1 Introduction and Motivation for Array-Based Sensing

While single optical fiber sensors proved effective for detecting strain and deformation in soft media, spatial localization of impacts requires distributed sensing across a defined area or volume. In mild traumatic brain injury (mTBI) modeling, resolving the mechanical events' location, directionality, and intensity necessitates multi-point measurement systems. This chapter outlines the evolution of the sensor array designs, from initial planar arrangements in hydrogel matrices to developing a four-layer silicone-based array to enable 3D impact detection.

4.2 Design and Fabrication of the 2D Sensor Array

The initial sensor array was designed as a 13 × 13 cm square frame accommodating orthogonally aligned sensors in two axes. Each axis incorporated eight sensors evenly spaced across the surface, forming a grid layout to capture planar deformation information. The frame was fabricated using ProBlack resin on a Figure 4 3D printer to ensure high resolution and dimensional stability.

Sensors were manually inserted into horizontal and vertical grooves along the grid lines. Once positioned, the array was embedded in a hydrogel matrix consisting of a 1:3 mixture of 6% gelatin and 0.6% agarose. This formulation was

chosen for its soft tissue-mimicking mechanical properties and optical clarity. Sensors remained suspended within the gel and fixed at both ends to maintain appropriate tension.

The purpose of this array was to establish fabrication feasibility, ensure mechanical compatibility between the sensors and the hydrogel, and observe whether an embedded network of sensors could be stabilized within a hydrated medium. It served as an intermediate step between individual sensor calibration and the development of multilayer silicone-based arrays.

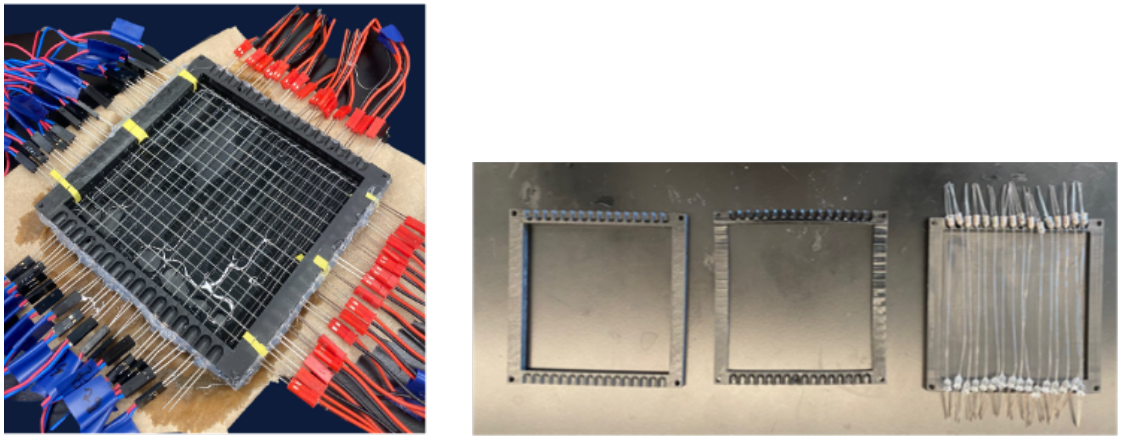

(a) 2D Model with sensor (b) Deconstructed 2D Model layers

Figure 4.1: Top-down view of 2D array frame showing sensor orientation and spacing.

The crossing points between orthogonal fibers were not physically connected; instead, they operated independently, each acting as an individual deformation sensor spanning the corresponding row or column. This approach enabled the system to detect impacts by monitoring which sensors registered voltage drops, allowing for early triangulation of impact locations based on signal patterns.

4.3 Limitations of Hydrogel as an Embedding Medium

Despite its compatibility with soft sensors, the gelatin-agarose hydrogel presented several practical limitations. The material was susceptible to dehydration, leading to volumetric shrinkage and sensor misalignment. Additionally, handling during mold filling and removal introduced mechanical stress to the gel structure, often displacing sensors or creating voids within the matrix. Repeated hydration cycles led to mold contamination and degradation of optical clarity. These complications impaired test reproducibility and posed challenges for long-term integration or multi-use applications. Ultimately, although the hydrogel system allowed for preliminary exploration of embedded sensor array behavior, it was unsuitable for repeatable or high-impact testing protocols. These observations motivated the transition to silicone-based arrays, which offered greater structural stability while maintaining compliance comparable to that of biological tissue.

4.4 Design and Proof-of-Concept of the Multilayer Silicone Array

The shift to a 3D-capable design led to the development of a multilayer array architecture composed of four stacked sensor layers embedded in silicone. A hexagonal cross-sectional geometry was selected to maintain uniform spacing and reduce signal blind spots. Each layer was spaced 10 mm apart vertically, and each layer contained eight sensors for a total of 32.

The mold was fabricated using ProBlack resin on a Figure 4 3D printer. Its

internal grooves ensured consistent fiber routing, while the open-top design enabled sequential sensor placement before casting. Once all sensors were aligned and tensioned across their respective slots, Ecoflex 00-30 silicone was poured into the mold in one continuous step, fully submerging the sensor matrix.

In the first iteration of this 4-layer model, the optical fibers were not yet cladded, which resulted in a complete loss of signal from all photodiodes due to the opacity of the silicone. After this, a second version was fabricated with cladded fibers using Wacker ELASTOSIL® RT 604. This significantly improved signal transmission, and successful responses were observed from the photodiodes when the model was manually pressed or tapped.

Although no structured test was conducted on this version, the primary goal was to evaluate the feasibility of a silicone volumetric distributed sensing configuration. Sensors from various layers responded to different tap intensities, supporting the use of the 4-layer format as a proof of concept for 3D sensor arrays.

An improved 4-layer model with an increased height of 80 mm is planned for future work. This configuration will include four sensors per layer and will be tested using a linear actuator. The actuator will incrementally increase the applied force to determine how sensor readings vary across layers and to assess depth-dependent sensitivity.

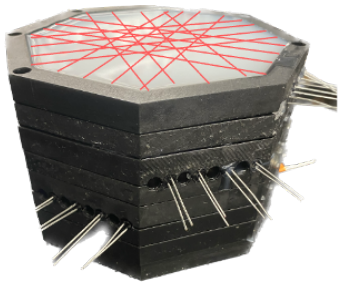

Figure 4.2: Cross-sectional schematic of the 4-layer hexagonal array design showing sensor routing and spacing.

4.5 Signal Loss Challenges and Shielding Approaches in Arrays

Although fiber cladding proved successful in the second iteration of the 4-layer model, the transition to silicone still presented challenges. Optical signal degradation remained a concern due to the cumulative effects of scattering and attenuation across longer fiber paths. While the manual tapping test confirmed that sensors across multiple layers were functional, no precise measurements could be collected due to the informal nature of the testing. In earlier hydrogel-based arrays, intersensor optical crosstalk and ambient light interference were addressed by applying metallic shielding paint to the photodiodes. This technique successfully improved signal clarity in planar applications. However, it did not address attenuation issues inherent to silicone-based embedding. These observations suggest improved emitter strength, an increased fiber diameter, or re-optimized cladding formulations in future volumetric array designs. While the signal was not lost entirely in the cladded version, the conditions under which sensor performance remains reliable still need to be explored through controlled dynamic testing.

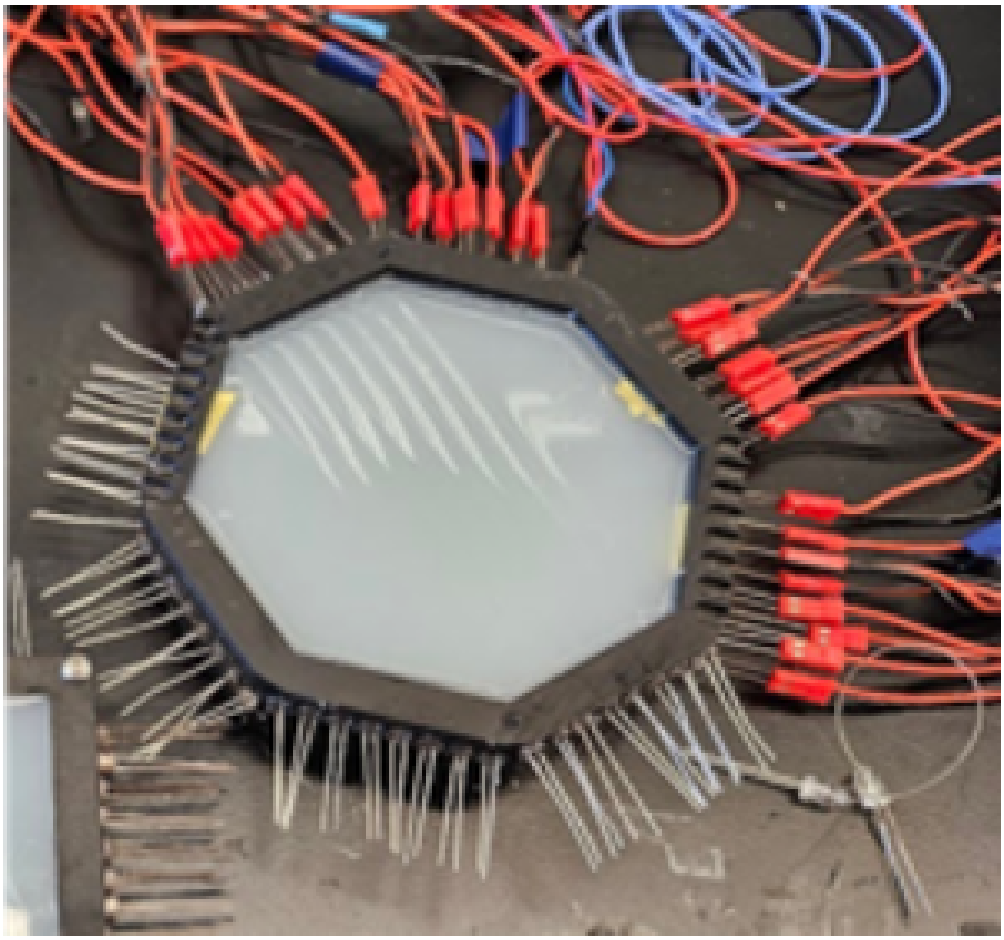

Figure 4.3: Image of embedded 4-layer silicone array showing fiber cladding and photodiode shielding.

CHAPTER 5

MECHANICAL TESTING AND IMPACT RESPONSE CHARACTERIZATION

5.1 Introduction

Before high-speed impact testing could be meaningfully conducted, evaluating the mechanical and electrical consistency of the fabricated optical fiber sensors under controlled loading conditions was critical. This chapter presents the results of compression and tapping tests to assess linearity, repeatability, and sensitivity across multiple sensors. These tests provided a controlled baseline and characterized both the mechanical stiffness and, more importantly, the voltage response of the sensors to externally applied forces.

5.2 Compression Test Results and Sensor Performance

To evaluate the performance and reproducibility of the optical fiber sensors under controlled mechanical inputs, a series of compression tests was conducted using the CellScale UniVert testing system. Four individually fabricated sensors were mounted in a custom 3D-printed resin holder designed to align and secure the optoelectronics without applying pre-strain. Each holder featured two press-fit indentations that matched the geometries of the LED and photodiode on both ends of the 11.25 cm-long sensor, ensuring that only the sensing segment of the fiber was in contact with the compressive surface. The compression tests were performed in force-controlled mode utilizing a 10 N load cell.

The testing protocol comprised five identical cycles, each involving a peak force of 5 N, a preload of 0.1 N, a stretch duration of 2 seconds, a hold period of 0.01 seconds, a recovery phase of 2 seconds, and a rest interval of 0.01 seconds. The sensor's voltage response was recorded via the DAQ system at a rate of 1 kHz, while force and displacement data were simultaneously logged by the UniVert at 100 Hz. To facilitate cycle-by-cycle comparison between mechanical input and optical output, all signals were time-synchronized using interpolation.

5.3 Trial Comparison Across Sensors

Figures 5.1 through 5.4 show the synchronized time-series comparisons for each sensor over the four analyzed cycles. For each trial, plots include force vs. time, displacement vs. time, voltage vs. time, and voltage vs. displacement. Mechanical inputs across all sensors were consistent, with force peaking at approximately 5 N and displacements ranging between 0.20 mm and 0.30 mm. Sensor 1 showed highly consistent voltage responses across cycles and trials. The voltage dropped steadily and returned to baseline at the end of each cycle. Overlay plots confirmed minimal trial-to-trial drift. Sensor 4 followed a similar trend, with clean, non-overlapping cycle curves and tightly grouped voltage responses, indicating stable optical alignment and good reproducibility. Sensor 2 showed larger inter-trial differences, particularly in signal amplitude. Notably, Trial 3 displayed a voltage trace consistently higher than the others, suggesting possible over-coupling or slight misalignment. Sensor 3 showed a large spread and nonlinear regions, indicating a less stable optoelectronic response, possibly due to insufficient contact, bending, or local delamination at the LED–fiber interface.

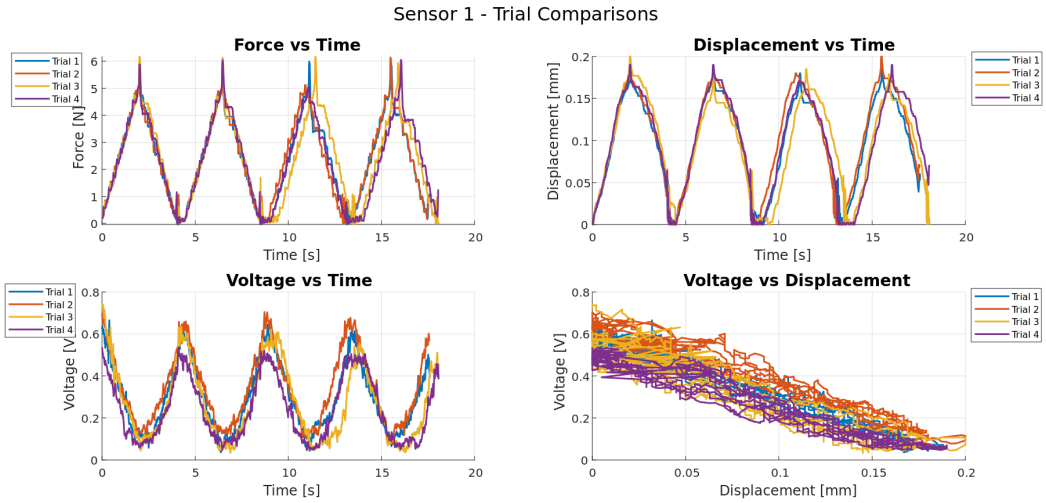

Figure 5.1: Sensor 1 – Trial Comparison Plots (Force, Displacement, Voltage, and Voltage vs. Displacement)

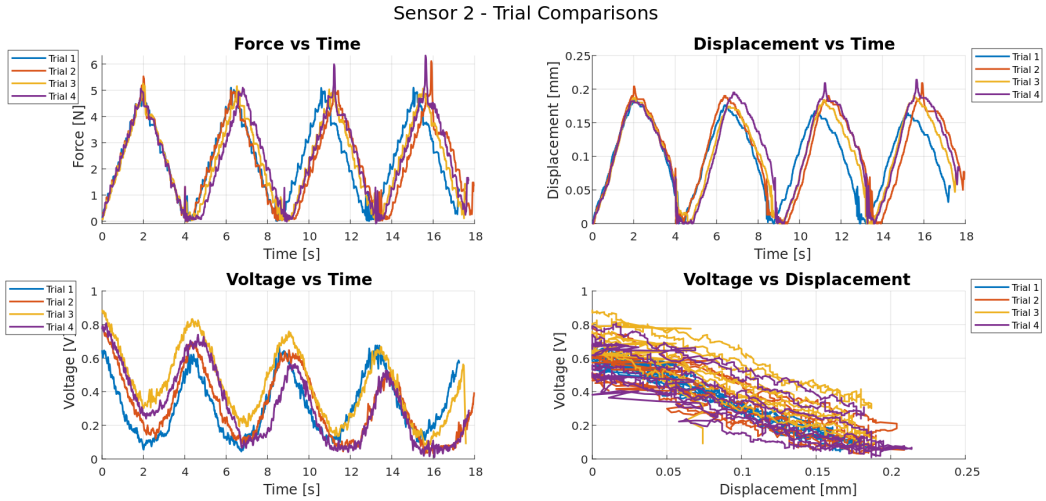

Figure 5.2: Sensor 2 – Trial Comparison Plots

5.4 Cycle-to-Cycle Δ Comparison

To quantify signal repeatability, voltage curves were normalized, and the delta (Δ) was computed for each cycle—the difference between maximum and minimum voltage. Figures 5.5 to 5.8 show the overlaid voltage vs. time curves with Δ regions highlighted, and Table 5.1 lists Δ values for each trial and cycle.

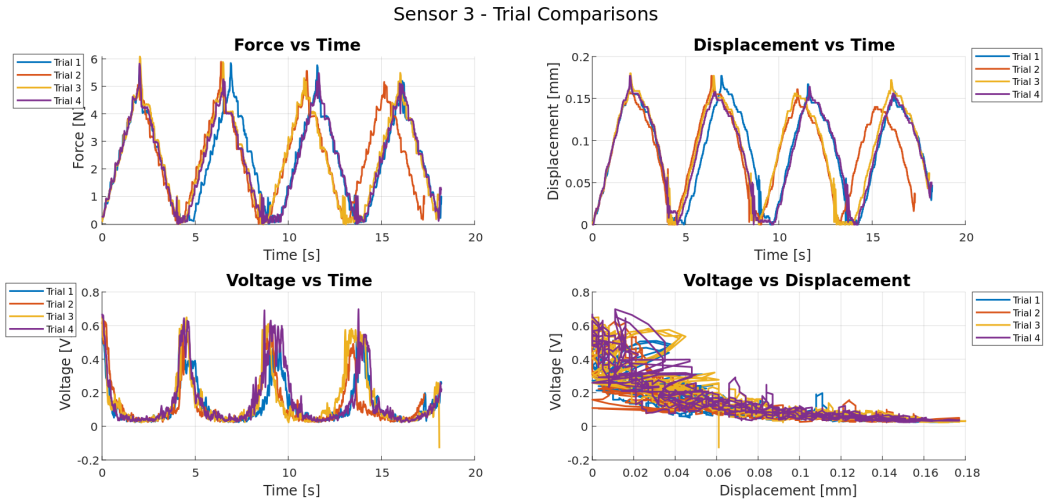

Figure 5.3: Sensor 3 – Trial Comparison Plots

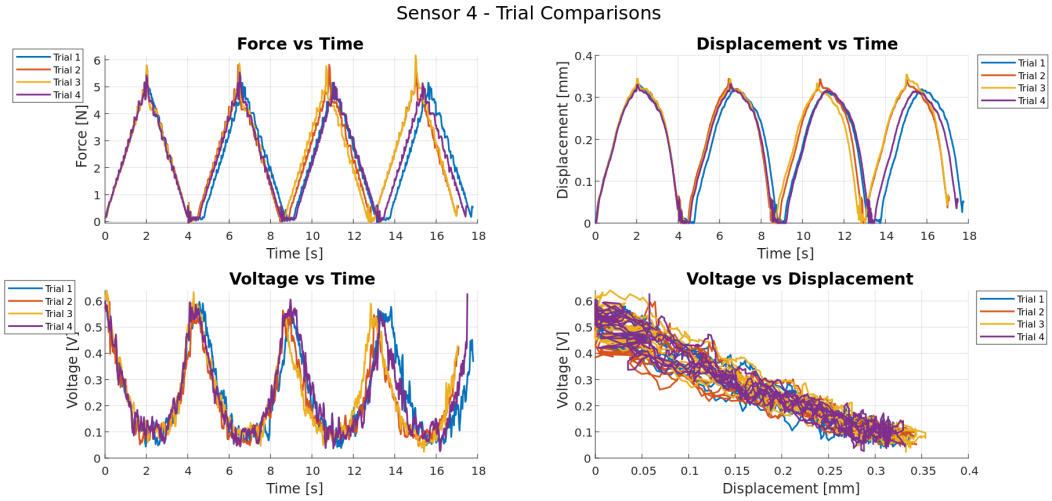

Figure 5.4: Sensor 4 – Trial Comparison Plots

Sensor 1 had an average $\Delta = 0.655$ V, showing moderate repeatability, with Trial 4 exhibiting slightly reduced amplitude. Sensor 2 exhibited the highest average $\Delta = 0.669$ V, and also the most fluctuation across cycles, reinforcing concerns about signal stability. Sensor 3 showed an average $\Delta = 0.654$ V, but with erratic baseline shifts and clipping. Sensor 4 had the lowest and most consistent Δ values (average $\Delta = 0.604$ V), demonstrating its superior cycle-to-cycle performance.

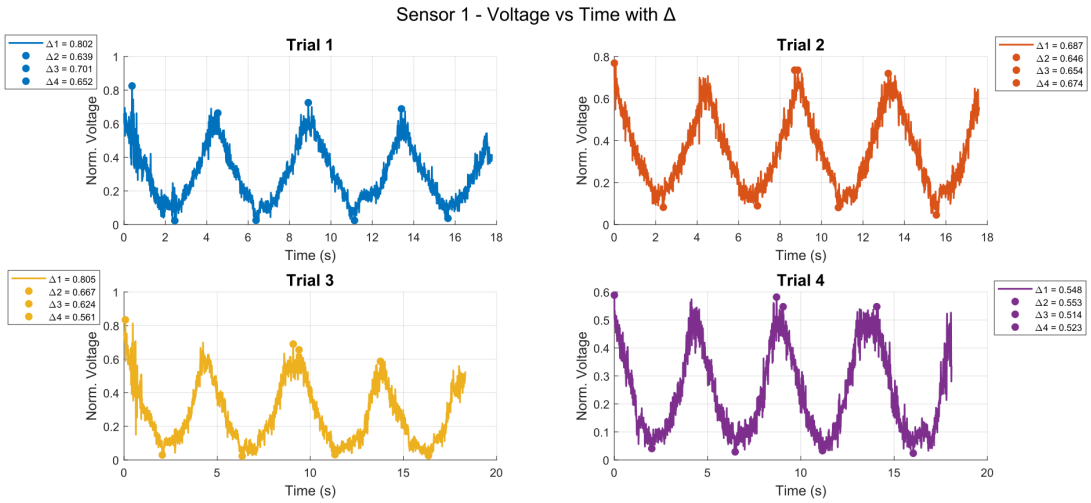

Figure 5.5: Sensor 1 – Voltage vs. Time with Highlighted)

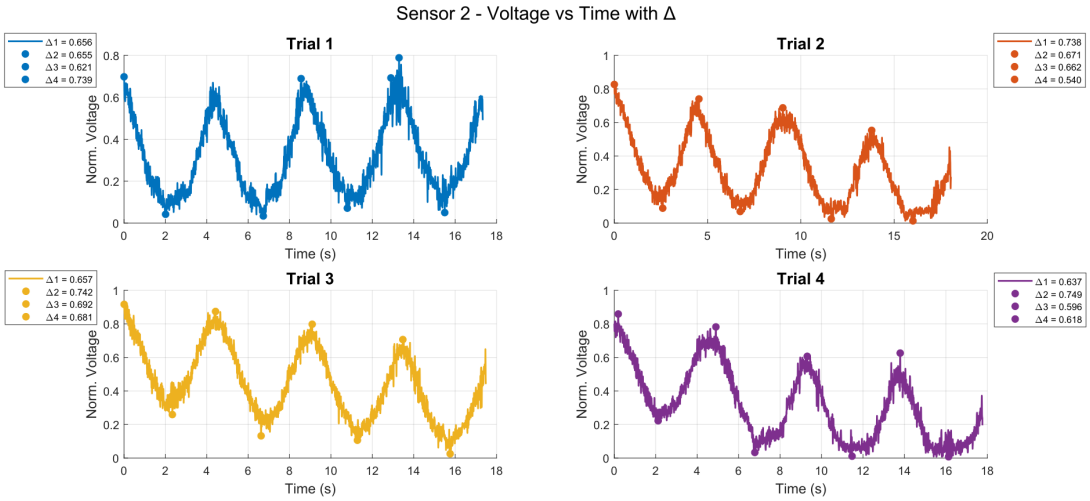

Figure 5.6: Sensor 2 – Voltage vs. Time with Highlighted

5.5 Voltage vs. Displacement Analysis

The voltage vs. displacement relationship, shown in Figures 5.9 to 5.12, captures how each sensor transduced mechanical compression into an optical response. These plots also include standard deviation (σ) error bars to quantify variability across cycles.

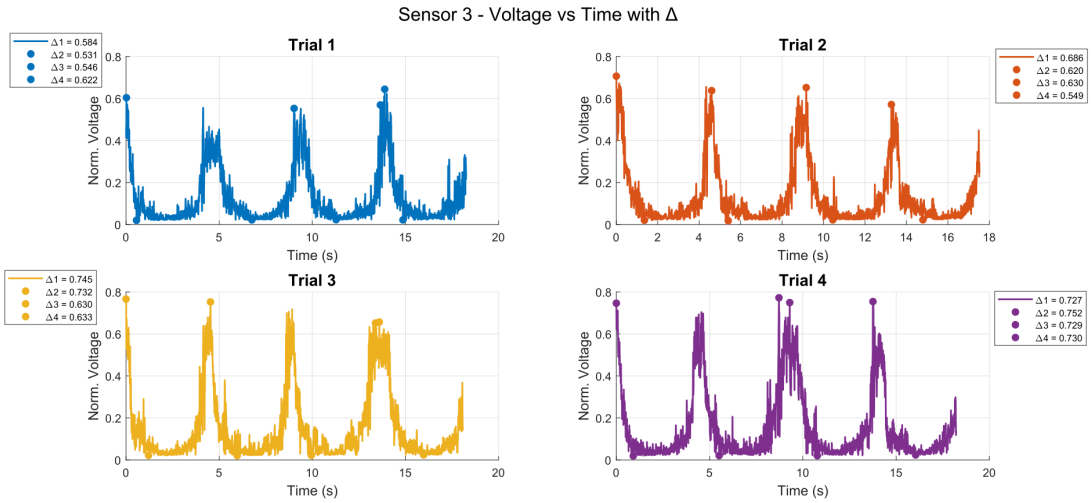

Figure 5.7: Sensor 3 – Voltage vs. Time with Highlighted

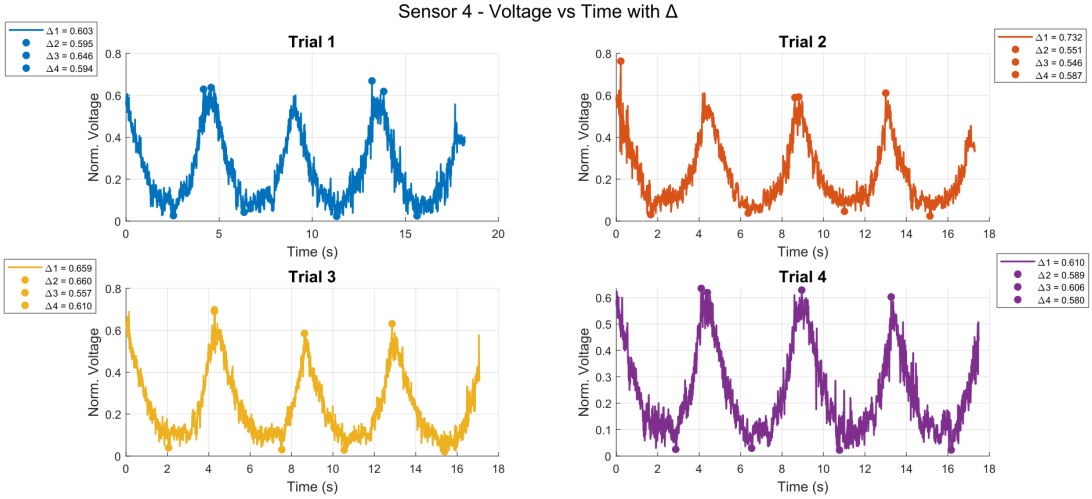

Figure 5.8: Sensor 4 – Voltage vs. Time with Highlighted

Sensor 1 exhibited a steady, near-linear voltage decrease from approximately 0.6 V to 0.2 V over 0.18 mm displacement. The average standard deviation across cycles was $\sigma = 0.0619$ V. Sensor 4 performed best overall with minimal signal noise and excellent linearity ($\sigma = 0.0451$ V), confirming it as the most mechanically and optically stable configuration.

Sensor 2 produced inconsistent slopes and showed wide vertical error bars

Table 5.1: Cycle-wise Δ values for each sensor (Cycles 2–5)

Sensor	**Trial**	Δ_2 (V)	Δ_3 (V)	Δ_4 (V)	Δ_5 (V)
Sensor 1	Trial 1	0.802	0.639	0.701	0.652
	Trial 2	0.687	0.646	0.654	0.674
	Trial 3	0.805	0.667	0.624	0.561
	Trial 4	0.548	0.553	0.514	0.523
Sensor 2	Trial 1	0.656	0.655	0.621	0.739
	Trial 2	0.738	0.671	0.662	0.540
	Trial 3	0.657	0.742	0.692	0.681
	Trial 4	0.637	0.749	0.596	0.618
Sensor 3	Trial 1	0.584	0.531	0.546	0.622
	Trial 2	0.686	0.620	0.630	0.549
	Trial 3	0.745	0.732	0.630	0.633
	Trial 4	0.727	0.752	0.729	0.730
Sensor 4	Trial 1	0.603	0.595	0.646	0.594
	Trial 2	0.732	0.551	0.546	0.587
	Trial 3	0.659	0.660	0.557	0.610
	Trial 4	0.610	0.589	0.606	0.580

Table 5.2: Average Δ value per sensor

Sensor	**Average Δ (V)**
Sensor 1	0.655
Sensor 2	0.669
Sensor 3	0.655
Sensor 4	0.604

(σ = 0.0992 V), indicating high noise or structural inconsistency. Sensor 3 demonstrated an early exponential decay followed by saturation, with moderate variation (σ = 0.0547 V), making it suitable only for narrow-range or binary detection tasks.

Table 5.3: Average standard deviation (σ) for each sensor across cycles

Sensor	**Cycle 2**	**Cycle 3**	**Cycle 4**	**Cycle 5**	**Average σ**
Sensor 1	0.0565	0.0549	0.0669	0.0693	0.0619
Sensor 2	0.1183	0.1079	0.0841	0.0864	0.0992
Sensor 3	0.0504	0.0546	0.0727	0.0411	0.0547
Sensor 4	0.0382	0.0390	0.0578	0.0455	0.0451

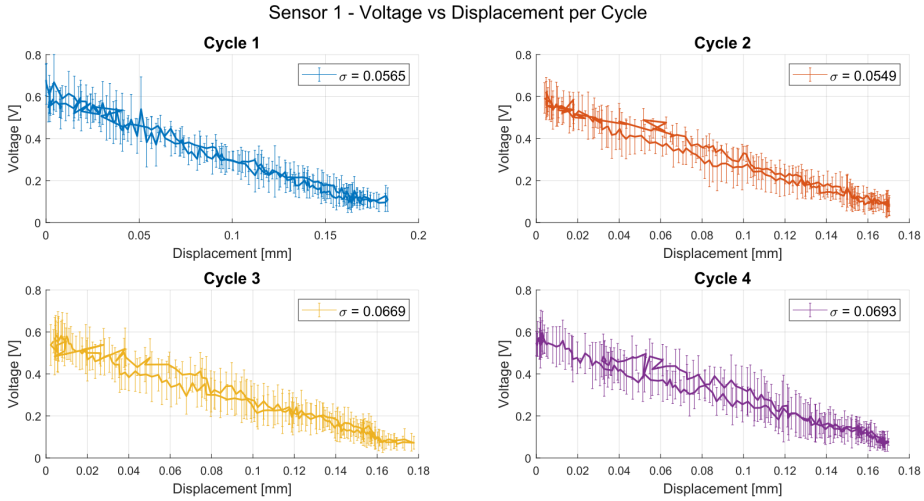

Figure 5.9: Sensor 1 – Voltage vs. Displacement per Cycle)

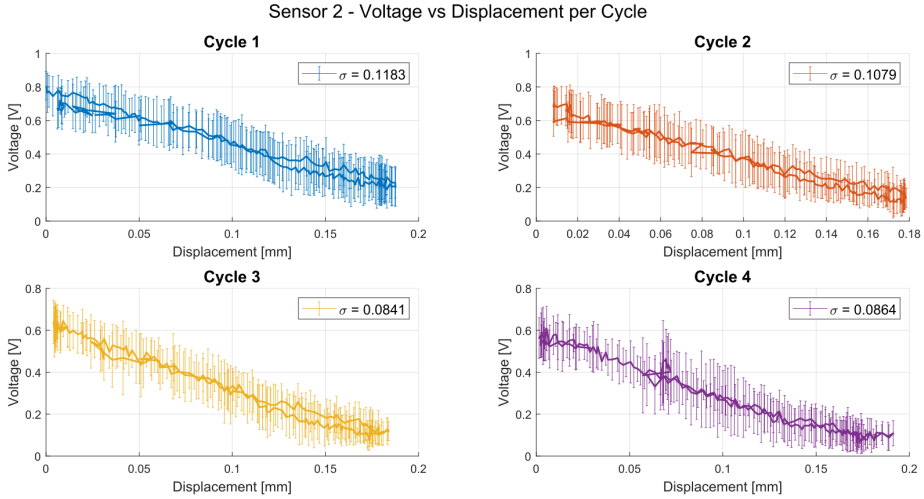

Figure 5.10: Sensor 2 – Voltage vs. Displacement per Cycle

5.6 Uniformity and Repeatability Assessment

Sensor 4 was the top performer in terms of consistency, linearity, and signal clarity. It had the lowest Δ and σ values and the cleanest alignment in all trial and cycle plots. Sensor 1 followed closely with reliable repeatability but slightly higher variability. Sensor 2 showed the most inconsistency across both voltage range and noise metrics, while Sensor 3's saturation behavior and abrupt

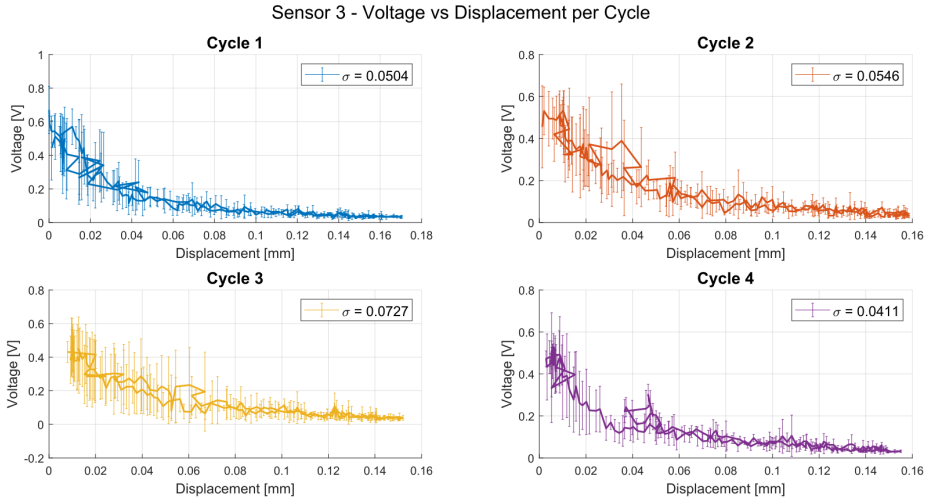

Figure 5.11: Sensor 3 – Voltage vs. Displacement per Cycle

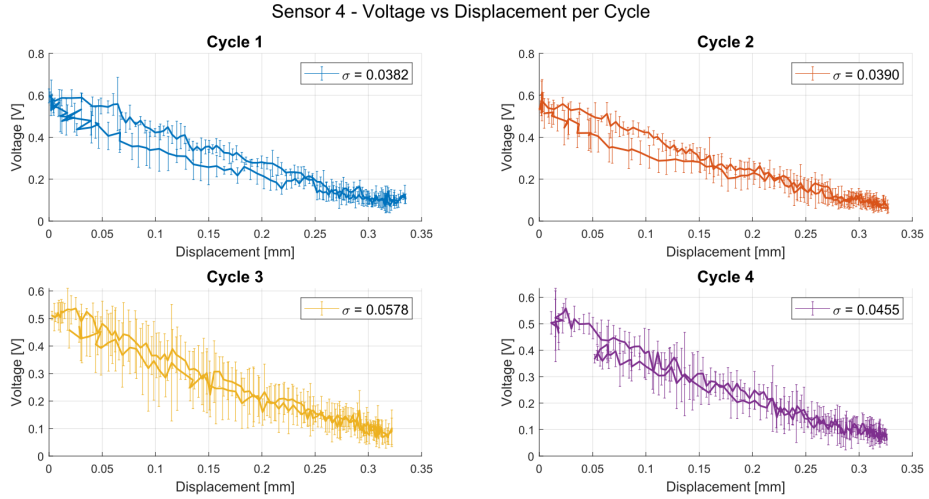

Figure 5.12: Sensor 4 – Voltage vs. Displacement per Cycle

response limited its utility to threshold-based applications.

These observations confirm the sensitivity of optoelectronic alignment and mechanical interfacing in the design of stretchable fiber sensors. The significant spread in performance despite identical fabrication conditions underscores the importance of precise integration and robust mechanical support.

CHAPTER 6

HIGH-SPEED IMPACT TESTING ON SYNTHETIC MODELS

6.1 Introduction

Following the successful mechanical characterization of the optical fiber sensors, high-speed impact testing was conducted to evaluate the real-time dynamic performance of the sensing system under ballistic and rapid mechanical loads. These tests are essential for validating whether the sensors can capture fast deformation events relevant to mild traumatic brain injury (mTBI) simulations. The experiments were conducted using synthetic hydrogel and silicone samples embedded with one or more sensors, each subjected to high-speed impacts from either a shotgun blast or a crossbow-launched projectile. Real-time voltage signals were collected using a high-sampling-rate data acquisition system and were synchronized with high-speed video recordings using an LED trigger signal.

6.2 Experimental Setup

All tests were performed using a high-speed data acquisition (DAQ) system operating at 500 kS/s, ensuring sufficient temporal resolution to capture transient deformation signals. Voltage readings from the photodiodes were recorded through a 32-channel National Instruments USB-6349 DAQ. An infrared LED illuminated the optical fiber, and the photodiode output was fed directly to the DAQ without amplification. For synchronization with high-speed video, an ex-

ternal LED marker was triggered during each impact event. The LED signal was simultaneously captured by both the camera and the DAQ, enabling alignment between visual footage and electrical signal traces. MATLAB was used to plot and analyze the voltage signals in real-time.

6.3 Ballistic Test – Hydrogel Model with Single Sensor

The first high-speed experiment was performed using a hydrogel probe embedded with a single optical fiber sensor. The hydrogel was molded into a cylindrical form and constructed from a 6% gelatin and 0.6% agarose blend to mimic soft tissue consistency. The sensor was cast directly into the matrix.

The impact was delivered using a 0.410 gauge shotgun round aimed at the hydrogel target. Upon projectile contact, the photodiode signal spiked sharply from its baseline (~3.9 V) and saturated at 4.0 V. Immediately after the impact, a series of oscillations was observed in the voltage signal, likely corresponding to the shockwave and recoil dynamics of the blast wave within the hydrogel. The LED marker was used to timestamp the moment of impact, which coincided precisely with the onset of the voltage spike.

The sensor exhibited a clear high-speed response, demonstrating its ability to register rapid and extreme deformation. However, the signal saturated quickly, indicating that stronger light sources or improved dynamic range may be required for future ballistic scenarios.

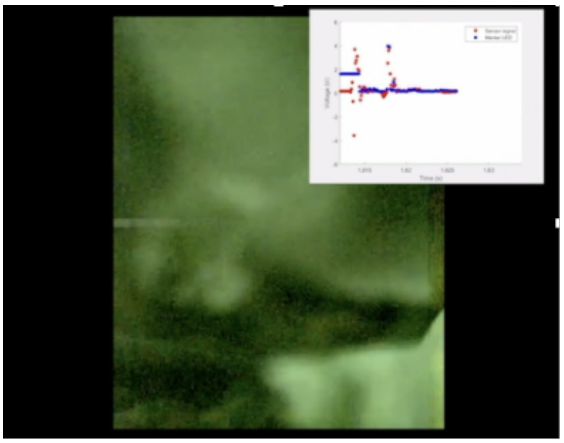

Figure 6.1: Voltage vs. Time graph for the hydrogel ballistic test with LED marker

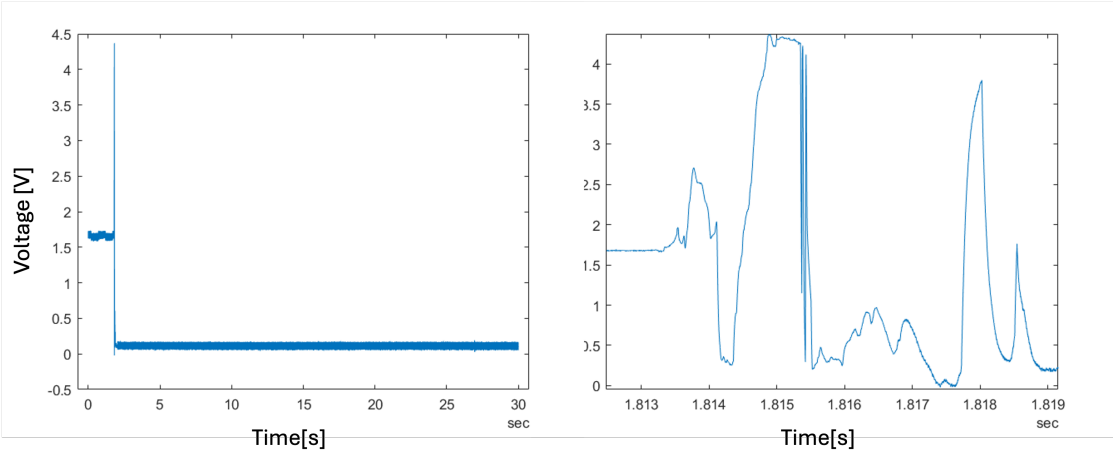

Figure 6.2: Voltage vs Time plot of high-speed ballistic impact to the sensor.

6.4 High-Speed Impact – Hydrogel Model with Single Sensor

A second high-speed test was performed using a silicone probe embedded with a single optical sensor. Ecoflex 00-30 silicone was selected for its compliance and similarity to soft biological tissue. The probe was subjected to a high-speed impact using a crossbow-launched arrow aimed at its center. The voltage signal remained stable at approximately 4.5 V before impact. At 3.62 seconds, as marked by the LED trigger, the signal dropped sharply to 3.5 V, followed by

damped oscillations similar in shape to those seen in the hydrogel test. These oscillations persisted for several milliseconds before the voltage stabilized. This test confirmed that the sensor could detect and recover from sharp deformation events in more mechanically stable media such as silicone. The dynamic range was slightly higher than in the hydrogel case, and the signal exhibited less saturation.

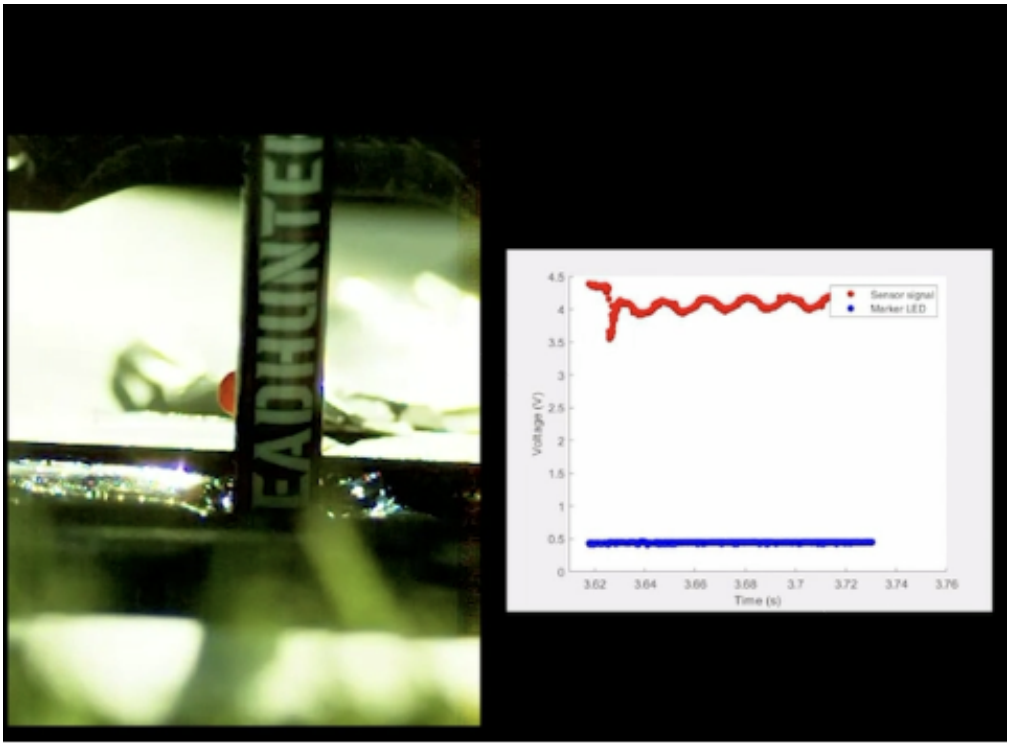

Figure 6.3: Voltage vs. Time graph for the hydrogel crossbow test of the high-speed impact with LED marker timestamp.

6.5 Multi-Sensor Impact Test – 3-Sensor Probe in Silicone

To further analyze impact propagation and inter-sensor dynamics, a three-sensor probe was fabricated using Ecoflex 00-30 silicone. The sensors were distributed across the surface of the probe at different locations to assess spatial response during high-speed impact. The test was again performed using a crossbow-launched projectile. All three sensors were powered and recorded simultaneously. The resulting Voltage vs. Time curves revealed a shared response profile among the sensors: each exhibited a drop in voltage coinciding with the moment of impact, but the timing and magnitude of the voltage change varied slightly by location. Sensor A showed the earliest voltage drop, consistent with its proximity to the impact site. Sensor B exhibited a delayed but more substantial signal change, suggesting wave propagation through the silicone medium. Sensor C showed a smaller and slower voltage shift, indicating reduced deformation or damping at its location. These results suggest that distributed optical fiber sensors embedded in soft tissue-mimicking materials can effectively capture both the onset and propagation of mechanical events across space and time.

6.6 Signal Behavior and Limitations in Dynamic Events

Across all high-speed synthetic tests, one of the key challenges encountered was the saturation of sensor signals during extreme deformation. In particular, the hydrogel-based ballistic test saturated the photodiode output nearly instantaneously, limiting the usable range of the response. While the silicone-based tests showed more controlled voltage shifts, the issue of limited dynamic range remains a concern. An unexpected phenomenon was observed during early test-

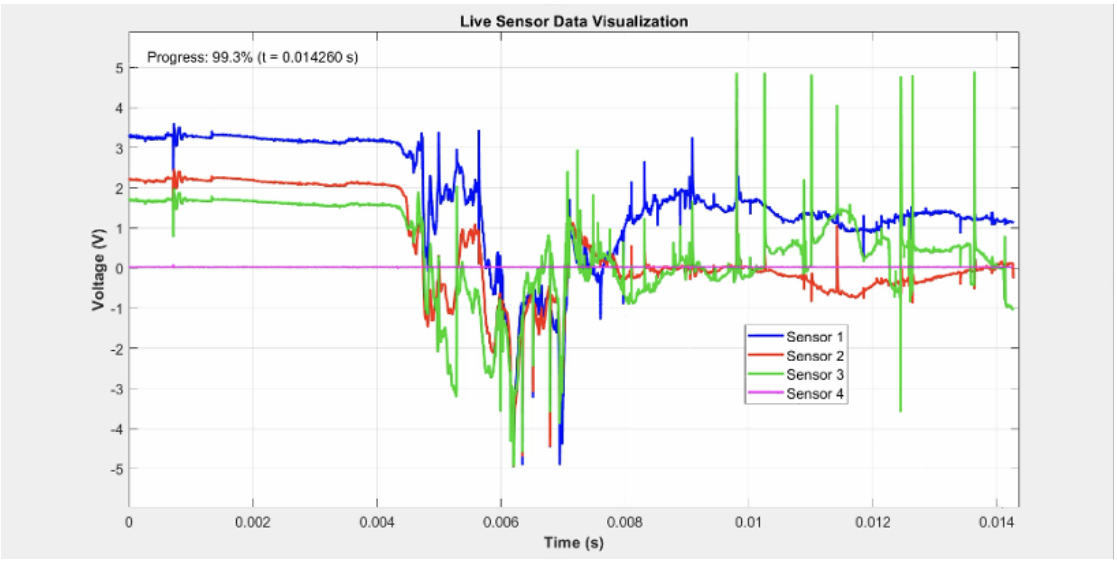

Figure 6.4: Overlaid Voltage vs. Time graph showing all three sensor responses.

ing: in some instances, the photodiode continued to output a saturated voltage even after the LED was disconnected. This unexpected behavior led to speculation about potential causes, including back-voltage buildup, residual current within the photodiode, or electrostatic charge accumulation. These observations suggest the need for further circuit-level investigations and possible improvements to signal conditioning in future designs.

CHAPTER 7

BIOLOGICAL MODEL INTEGRATION AND EXPERIMENTAL VALIDATION

7.1 Motivation and Context

Sheep brains are widely used in neurological research as they present an effective anatomical and mechanical model for the human brain, given their similar cortical folding, overall mass, and soft tissue properties [4]. Their availability and ease of handling make them a practical choice for studying brain-device interactions outside clinical or in vivo environments [6]. In this work, we used the sheep brain as a biological testbed to evaluate whether the optical fiber sensors, initially designed for synthetic substrates, could securely adhere to the tissue, maintain signal integrity, and function reliably when interfaced with soft biological tissue. This assessment allowed us to evaluate sensor performance and its potential for anatomical embedding in direct contact with tissue. The objective of this phase was to determine whether the optical fiber sensors could securely attach to the soft biological substrate, maintain functional signal output, and withstand realistic handling. Specifically, this series of experiments focused on both surface-mounted and partially inserted sensors on preserved sheep brains, including attempts to embed the entire sensor-brain assembly within a skull cavity.

The preserved brains used in these tests were obtained from Carolina Biological and stored in Carolina's Perfect Solution[3], a fixative renowned for preserving tissue structure without blood or harsh chemicals. This setup enabled direct mechanical experimentation in a controlled benchtop environment. This chap-

Figure 7.1: Overview image of preserved sheep brain setup and printed sensor holder.

ter presents detailed results from the surface attachment, hydration behavior, and brain-in-skull integration tests, along with the practical and optical limitations encountered during the experiments.

7.2 Brain-on-Bench Model Preparation

The preserved sheep brains were ordered with and without dura mater, providing options for surface accessibility. No additional preparation involving chemical treatment or rinsing was performed, and the samples were used directly after brief storage in sealed containers. To prevent sensor displacement and maintain anatomical integrity during handling, a custom oval-shaped holder was designed using ProBlack resin on a Figure 4 3D printer. The oval geometry closely matched the contour of the sheep brain, minimizing internal movement and allowing repeatable placement. To stabilize the sensors and apply appro-

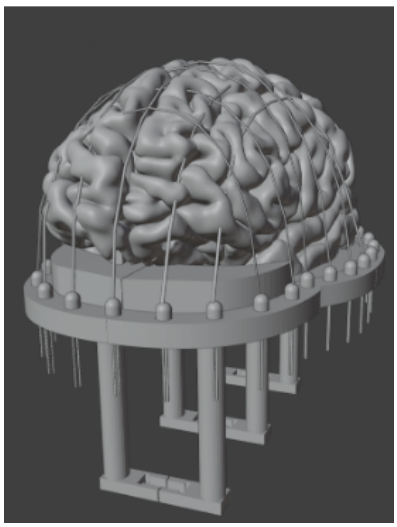

(a) CAD file of Sheep brain with the sensor grid attached to the holder

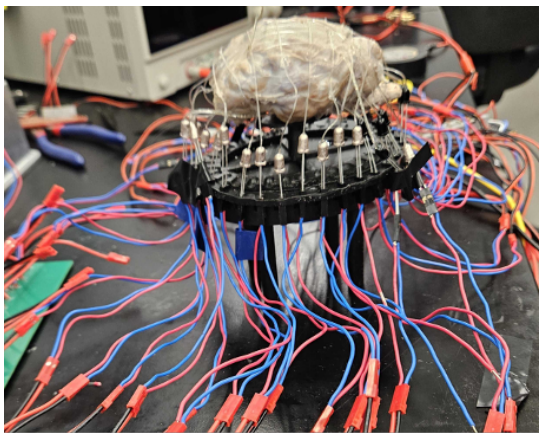

(b) Brain Model Setup

Figure 7.2: CAD rendering and assembled image of the tensioning system used for brain-on-bench experiments. The rigid oval holder constrains lateral motion, while the flexible contouring band printed in Rubber 65 - maintains consistent contact between the sensor and brain surface.

priate tension across the brain surface, a flexible contouring band was printed using Rubber 65 material. The band fits snugly over the resin base, allowing controlled contact between the sensor array and the brain surface. This adjustment mechanism proved helpful in managing slight dimensional differences across brains and sensor arrays.

7.3 Sensor Attachment and Integration

This integration represents one of the first experimental attempts to directly adhere stretchable optical fiber sensors to preserved neural tissue using simple adhesives while maintaining a measurable signal. The success of this surface-mounting approach, without encasing the sensor in additional embedding ma-

terial, marks a significant step toward anatomical compatibility and system miniaturization for in situ deformation sensing.

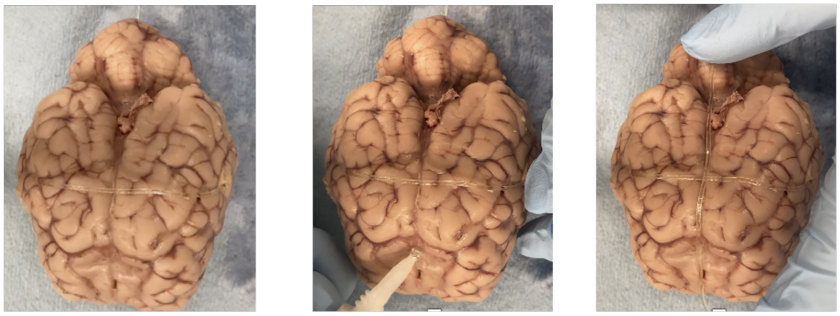

Figure 7.3: Sensor mounting procedure on the brain surface. (a) Sensor alignment before fixation. (b) Application of Gorilla Super Glue at anchor points. (c) The final seated position of the optical fiber sensor is across the brain curvature.

Sensor placement was performed with special attention to anatomical features, curvature, and mechanical contact. Sensors were glued directly to the brain's surface using Gorilla Super Glue. The adhesive was applied at two discrete anchor points, one at each end of the sensor, to avoid excessive stiffness along the length of the optical fiber. The fibers were passed through the band to improve alignment and limit motion. The placement process followed the design and methodology, which included progressive steps for positioning, holding, gluing, and releasing the sensors. Special care was taken to avoid areas with excessive curvature or variability in surface hydration. Once glued, the sensors remained positioned throughout mechanical inspection and voltage testing. Sensor alignment was confirmed visually, and initial voltage output was recorded to assess baseline functionality.

7.4 Hydration-Induced Sensor Swelling

This phenomenon has important implications for the long-term viability of the current sensor design in biological environments. Without barrier coatings or modified cladding materials, prolonged exposure to biological fluids or fixatives may compromise mechanical and optical performance. Future efforts should explore hydrophobic coatings or low-permeability elastomers to mitigate this issue.

An unexpected complication arose during initial attempts to store the brain overnight while preserving sensor positioning. After submerging the brain with attached sensors in Carolina's Perfect Solution®, the sensors were found loose and misaligned the following day. Initially, this was assumed to be caused by dehydration and the shrinkage of biological tissue. However, further investigation revealed that the optical fibers had absorbed liquid from the storage solution and swelled.

A controlled experiment was performed using a 10 cm segment of cladded fiber submerged overnight. Upon removal, the fiber had increased in length by approximately 9 mm. This swelling was consistent across repeated trials and was attributed to absorption of the storage solution by the silicone cladding or the thermoplastic polyurethane (TPU) core. The swelling compromised the tension in pre-mounted fibers, leading to signal instability and drift in previously calibrated sensors.

This result suggests that fiber composition and cladding selection must be reconsidered for long-term biological deployments. Protective coatings or hydration barriers may be necessary in future designs.

7.5 Brain-in-Skull Integration Attempt

This test was performed as a preliminary validation of anatomical integration in a constrained cavity, rather than a repeatable protocol. Only one preserved sheep brain was used, and the experiment was not repeated after observing voltage saturation. Nonetheless, it provided critical insight into mechanical strain during placement and photodiode behavior under pre-load.

7.6 Brain-on-Bench Model Preparation

(a) Sheep brain inside Sheep skull

(b) Sheep brain inside Sheep skull with sensor embedded

Figure 7.4: Brain-in-skull integration setup showing sensorized sheep brain placed within the cranial cavity. Sensors are secured using a combination of adhesive and needle-guided insertion. Voltage saturation behavior was observed in several sensors during placement.

A separate test was performed to evaluate the feasibility of inserting the sensorized brain into a skull cavity. The sheep skull was prepared by removing

loose tissue and allowing visual access to the brain chamber. A single preserved sheep brain was then equipped with four sensors: three surface-mounted sensors placed on the X, Y, and Z axes, and one internal sensor inserted into the brain tissue using a 14-gauge needle as a guiding channel. Once in position, the remaining segments of the fiber were glued into place to improve tension across the surface. Upon placement of the brain into the skull, several sensors began showing unusual baseline voltages approaching the 5 V saturation limit. In one particular case, a sensor remained saturated even after the LED source was disconnected. This unexpected behavior led to several hypotheses, including internal signal interference, back-voltage effects, or accumulated electrostatic charge within the photodiode. Despite several repositioning attempts and rechecks of the circuit, the sensor response remained unreliable. As a result, the test could not be completed, and no dynamic loading was applied. However, the anomalous saturation behavior raised critical questions about environmental sensitivity and circuit robustness when operating in constrained biological cavities.

CHAPTER 8

DISCUSSION AND FUTURE WORK

8.1 Synthesis of Findings

This thesis presented the development, characterization, and experimental validation of a stretchable optical fiber sensor system for real-time impact detection in soft and biological materials. A cohesive evaluation of the sensor system was achieved through a stepwise investigation beginning with fabrication and calibration, progressing through array integration and mechanical testing, and culminating in biological model experiments. The sensors demonstrated moderate repeatability under compressive loading, with performance differences across devices attributed to fabrication alignment and optical coupling. The sensors reliably captured voltage changes corresponding to mechanical deformation when embedded in soft media such as silicone and hydrogel. Integration into preserved sheep brains further confirmed their applicability in biologically relevant contexts, although limitations such as swelling, saturation, and optical variability emerged.

8.2 Limitations and Technical Challenges

Several limitations were identified throughout the development and testing phases:

Signal Variability and Reproducibility Under Compression: Compression tests revealed that although the sensors responded consistently to load cycles in

general, there was variability in signal amplitude and repeatability from baseline between sensors and trials. Factors such as minor misalignments, optical coupling efficiency, and sensor delamination likely contributed to these differences, highlighting the need for tighter integration control during fabrication and setup.

Swelling of Optical Fibers in Hydrated Environments: When submerged in preservation fluids, the optical fibers exhibited length expansion due to fluid absorption. This altered baseline tension and degraded sensor performance over time. Mechanical Pre-Strain and Signal Saturation in Anatomical Cavities: Sensors inserted into confined biological structures, such as a sheep skull, resulted in unexpected pre-strain and baseline saturation, potentially due to mechanical compression or trapped voltage at the photodiode.

Absence of Real-Time Localization Framework: Although sensors effectively captured impact signatures, the thesis did not develop or implement a real-time spatial localization algorithm beyond exploratory LASSO regression in 2D array tests. These limitations offer clear design targets for refinement in future sensor systems.

8.3 Addressing Gaps and Clarifying Performance

A clearer comparative framework between environments was introduced to strengthen the interpretation of the sensor's robustness across conditions. Compression tests showed moderate repeatability and signal stability across most sensors, but also revealed differences in voltage amplitude and linearity that were influenced by optical alignment and mechanical coupling. These varia-

tions emphasize the importance of refined integration practices to ensure consistent performance. Differences in signal behavior between hydrogel and silicone, such as smoother oscillatory damping in the latter, highlight the role of embedding media in shaping dynamic response. Furthermore, biological tests showed how swelling, tissue compliance, and photodiode shielding influenced sensor accuracy. These comparisons help contextualize the system's reliability across use cases and outline specific conditions under which performance may degrade or remain stable.

8.4 Localization Framework and Algorithmic Roadmap

While complete 3D spatial localization was not implemented in this work, initial progress was made using a 2D LASSO regression model. This method was tested on a 24-sensor matrix and later applied to a hydrogel-based array, where impacts and touch stimuli were detected as heat maps. Lighter shading in the matrix output corresponded to higher voltage changes, indicating more substantial localized deformation. The rationale for selecting LASSO regression over more complex neural networks was its computational efficiency and ease of interpretability. This approach could be scaled using sparse matrix interpolation for a volumetric system such as a dodecahedron sensor array. However, this would require a fully realized 3D sensor platform, which is beyond the current hardware implementation.

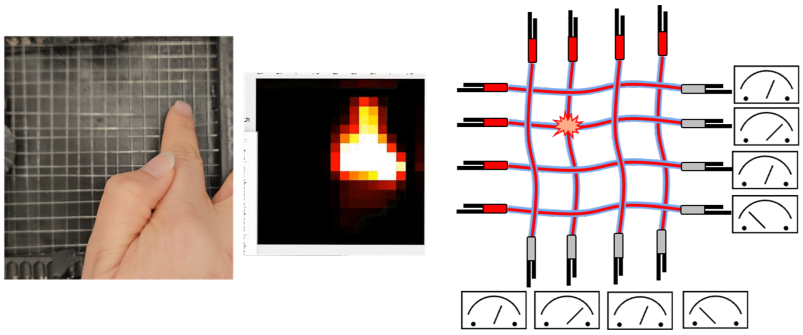

Figure 8.1: Applied concept of localization using LASSO regression as a heatmap. The brighter the color of the pixel, the higher the change in voltage.

8.5 Future Work

Several avenues for advancement have emerged from the findings: Biological Replication with Improved Stability: The brain-in-skull test will be replicated to examine signal saturation further and identify whether sensor swelling or circuit behavior is responsible. Hydration Control and Sensor Encapsulation: Alternative cladding materials or barrier coatings should be tested to mitigate liquid absorption and maintain mechanical tension. High-Speed Actuated Loading: A planned 80 mm four-layer silicone model will be tested using a linear actuator to evaluate depth-dependent sensitivity and inter-layer response systematically. Localization and Machine Learning Integration: To reduce training time, the existing LASSO framework will be extended into 3D configurations using coordinate mapping techniques or low-parameter convolutional networks. Cavitation and Shockwave Studies: Additional tests may examine whether the sensor system can detect internal cavitation events or rapid pressure wave propagation inside brain-mimicking materials.

8.6 Conclusion

This work demonstrated that flexible optical fiber sensors can be fabricated, calibrated, embedded, and validated for detecting dynamic mechanical events across soft synthetic and biological substrates. While several technical challenges remain, including signal saturation and integration with anatomical environments, the system shows strong potential for use in soft robotics, wearable diagnostics, and TBI research. The results establish a strong platform for the continued development of intelligent, distributed deformation sensing in biologically relevant systems.

BIBLIOGRAPHY

[1] H. Bai et al. “Stretchable distributed fiber-optic sensors”. In: *Science* 370 (2020), pp. 848–852.

[2] Silvia Budday, Paul Steinmann, and Ellen Kuhl. “Physical biology of human brain tissue: Nonlinear material behavior with damage and failure”. In: *Acta Biomaterialia* 10.10 (2015), pp. 4912–4925.

[3] Carolina Biological Supply Company. *Carolina’s Perfect Solution® Preserved Specimens – Safety Data and Handling Guidelines*. Accessed 2025.

[4] M. A. Cuddihy and J. O. Winter. “Biomimetic models of the brain for in vitro studies of central nervous system function and disease”. In: *Tissue Engineering Part B: Reviews* 16.1 (2010), pp. 29–42.

[5] B. Fehily and M. Fitzgerald. “Repeated Mild Traumatic Brain Injury: Potential Mechanisms of Damage”. In: *Cell Transplantation* 26 (2017), pp. 1131–1155.

[6] D. M. Geddes and R. S. Cargill. “An in vitro model of neural trauma: device characterization and calibration”. In: *Annals of Biomedical Engineering* 29.5 (2001), pp. 390–397.

[7] A. Ghatak and K. Thyagarajan. *Introduction to Fiber Optics*. Cambridge University Press, 1998.

[8] C. C. Giza and D. A. Hovda. “The Neurometabolic Cascade of Concussion”. In: *Journal of Athletic Training* (2001).

[9] Q. Guo et al. “Hydrogel-based materials for biomedical applications: A review”. In: *Journal of Materials Chemistry B* 9.33 (2021), pp. 6679–6704.

[10] R. H. Heisser et al. “Valveless microliter combustion for densely packed arrays of powerful soft actuators”. In: *Proceedings of the National Academy of Sciences* 118 (2021), e2106553118.

[11] A. D. Kersey. “A review of recent developments in fiber optic sensor technology”. In: *Optical Fiber Technology* 2.3 (1996), pp. 291–317.

[12] A. I. King et al. “Mechanisms of Head Injury”. In: *Proceedings of the IRCOBI Conference*. 2003.

[13] R. R. Levin and R. R. Diaz-Arrastia. “Diagnosis, prognosis, and clinical management of mild traumatic brain injury”. In: *The Lancet Neurology* 14.5 (2015), pp. 506–517.

[14] K. Luo, G. Subhash, and D. E. Spearot. “On shockwave propagation and attenuation in poly(ethylene glycol) diacrylate hydrogels”. In: *Journal of the Mechanical Behavior of Biomedical Materials* 118 (2021).

[15] W. Lv et al. “mTBI-Induced Systemic Vascular Dysfunction in a Mouse mTBI Model”. In: *Brain Sciences* 12.2 (2022), p. 232.

[16] D. Marcuse. “Loss analysis of single-mode fiber splices”. In: *The Bell System Technical Journal* 55.6 (1976), pp. 937–955.

[17] D. F. Meaney et al. “Biomechanical Modeling of Brain Injury: Beyond the Conventional Paradigms”. In: *Annals of Biomedical Engineering* (2014).

[18] L. Angela Mihai et al. “A comparative study of hyperelastic models for brain tissue”. In: *Journal of the Mechanical Behavior of Biomedical Materials* 46 (2015), pp. 1–10.

[19] A. R. Rabinowitz and T. K. Watanabe. “Pharmacotherapy for Treatment of Cognitive and Neuropsychiatric Symptoms After mTBI”. In: *Journal of Head Trauma Rehabilitation* 35.1 (2020), pp. 76–83.

[20] S. Rowson and S. M. Duma. "Development of the STAR Evaluation System for Football Helmets". In: *Annals of Biomedical Engineering* (2011).

[21] H. Souri et al. "Wearable and Stretchable Strain Sensors: Materials, Mechanisms, and Applications". In: *Advanced Intelligent Systems* (2020).

[22] E. Udd and W. B. Spillman. *Fiber Optic Sensors: An Introduction for Engineers and Scientists*. John Wiley & Sons, 2011.

[23] Q. Wang et al. "Flexible and wearable fiber-optic sensors for real-time monitoring of biomechanics and physiological signals". In: *Advanced Functional Materials* 29.22 (2019), p. 1807569.

[24] L. C. Wu et al. "Detection of American Football Head Impacts Using Wearable Sensors". In: *IEEE Transactions on Biomedical Engineering* (2016).

[25] P. A. Xu et al. "Optical lace for synthetic afferent neural networks". In: *Science Robotics* 4 (2019), pp. 1–10.

[26] H. Zhao et al. "Optoelectronically innervated soft prosthetic hand via stretchable optical waveguides". In: *Science Robotics* 1 (2016), eaai7529.

[27] H. Zhao et al. "Optoelectronically innervated soft prosthetic hand via stretchable optical waveguides". In: *Sci. Robot.* 1 (2016), eaai7529.